
CHALMERS
UNIVERSITY OF TECHNOLOGY

# An equivalent circuit model for swelling in Prismatic Lithium-ion cells

## Investigation of the pressure change dependence on the state-of-charge and charging rate, and model development for a Lithium-ion battery using an equivalent circuit.

*Master of Science Thesis*

Gingsjö Erik
erikgin@student.chalmers.se
M.Sc. Physics, Chalmers University of Technology

Harish Poshith
poshith@student.chalmers.se
M.Sc. Mobility Engineering, Chalmers University of Technology

Department of Electrical Engineering
*Division of Electric Power Engineering*
CHALMERS UNIVERSITY OF TECHNOLOGY
Göteborg, Sweden 2023
Report No.

# An equivalent circuit model for swelling in Prismatic Lithium-ion cells

## Investigation of the pressure change dependence on the state-of-charge and charging rate, and model development for a Lithium-ion battery using an equivalent circuit.

GINGSJÖ Erik

HARISH Poshith

Department of Electrical Engineering
*Division of Electric Power Engineering*
CHALMERS UNIVERSITY OF TECHNOLOGY
Göteborg, Sweden 2023

**An equivalent circuit model for swelling in Prismatic Lithium-ion cells**
Investigation of the pressure change dependence on the state-of-charge and charging rate, and model development for a Lithium-ion battery using an equivalent circuit.

Gingsjö Erik
Harish Poshith



Department of Electrical Engineering
*Division of Electric Power Engineering*
CHALMERS UNIVERSITY OF TECHNOLOGY
SE–412 96 Göteborg
Sweden
Telephone +46 (0)31–772 1000

Cover:
Lithium-ion battery

Chalmers Bibliotek, Reproservice
Göteborg, Sweden 2023

**An equivalent circuit model for swelling in Prismatic Lithium-ion cells**
Investigation of the pressure change dependence on the state-of-charge and charging rate, and model development for a Lithium-ion battery using an equivalent circuit.
GINGSJÖ Erik
HARISH Poshith
Department of Electrical Engineering
Division of Electric Power Engineering
Chalmers University of Technology

## Abstract

In this thesis, the expansion behavior of a Prismatic Lithium-ion cell is investigated via its external pressure changes. Experiments were done for 0% to 100% state-of-charge for both charge and discharge at various charging rates from 0.05C to 1.2C.

An equivalent circuit with a single resistance was used to model the pressure behavior during charging, where the modeled resistance can be understood as a mechanical resistance of the cell casing to expand. It was shown to exhibit a clear trend for charging rate as well as state-of-charge, with values becoming bigger with both increasing charging rate and state-of-charge up to 0.5C. The model was evaluated for 0.3C with the absolute relative error between the modeled and experimental result being around 1% after 5% to 100% state-of-charge. Data from two research articles with similar pressure change experiments were used to validate the model. The first, [1], used charging rates comparable to those used in this thesis, and the other, [2], used charging rates above 1C. For the former, the modeled resistance values showed similar trends as presented here. For the latter however, the resistance values instead decreased with both state-of-charge and increasing charging rate, which was assumed to be due to lithium plating at higher state-of-charge at the higher charging rates as well as due to thermal effects.

**Keywords: Li-ion cell, Cell swelling, Equivalent circuit model, Pressure response, Prismatic Li-ion cell**

## Acknowledgements

This thesis work was carried out at the Cell Simulation Group in Volvo GTT. It was presented in and graded by the Department of Electrical Engineering at the Chalmers University of Technology.

We are grateful to the assistance from the following people. It would have been difficult to complete the thesis work without them.

- Niladri Roy Chowdhury from Volvo GTT supervised and mentored us throughout this thesis work by guiding us whenever we were confused with theory, model development, and validation.
- Gustav Giske supported and instructed us throughout the process of the experimental set-up and conduction of experiments. Praveen Raju Hasabavi also shared his knowledge and time for the safe and successful completion of the experiments. Both of them were from Volvo GTT as well.
- The members of the Cell Simulation team who advised and encouraged us.
- Torbjörn Thiringer from Chalmers University of Technology who was the examiner for this thesis work. He also provided the experimental test-rig and sensors that we used and held hands throughout the project work, providing vital feedback on how the experiments were run.

We thank all the people mentioned above. Special gratitude to Volvo GTT and Chalmers University of Technology for providing the opportunity to learn and grow.

Finally, we thank our family and friends for their encouragement and boosting of our confidence.

Gingsjö Erik
Harish Poshith
Göteborg, Sweden, 2023

# Contents

# Chapter 1

# Introduction

Recently there has been a worldwide spike in the usage of *Lithium-ion*(Li-ion) batteries for numerous applications. Where one of the largest single applications is in the transport industry (See figure 1.1), in *battery electric vehicles* (BEVs) and *hybrid electric vehicles* (HEVs). Nowadays BEVs and HEVs are preferred over conventional *Internal combustion vehicles* (ICVs), mainly due to less pollution, less noise, and so on[3]. The increased price and supply shortage of fuel for ICVs offer yet other explanations. The electric car also has significantly fewer components in its power train than a conventional ICV, which increases reliability and reduces maintenance frequency, whereas conventional cars have an issue of strict regular engine maintenance followed by a raised replacement and repair cost of spare parts[4]. Moreover, automobile manufacturers are focusing on electric drive systems for their improved efficiency and reduced operational costs [5].

The European Commission has strict rules regarding the amount of pollutants in the exhaust emission from ICVs [6]. BEVs can meet the standards of the current regulations with efficient machines [4] [7]. Li-ion batteries are used in them because they have better cycle stability, high power and energy density, safety, etc, When compared to other battery varieties [8] [9]. The cost of mass production of the batteries is also reasonable [10], and their usage causes less harm to the environment [11].

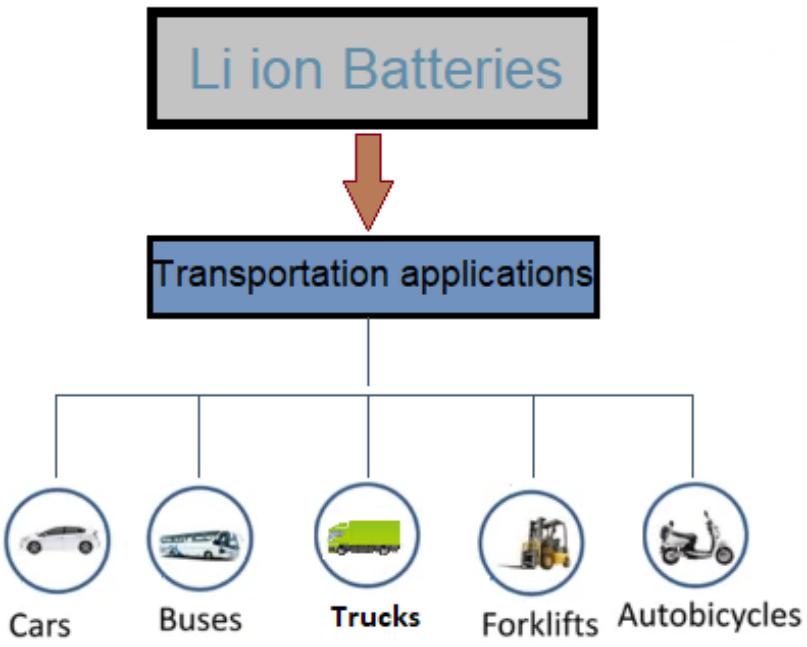


Figure 1.1: Li-ion batteries in Automobile industry

However, electric vehicles have drawbacks such as an increased price, long charging time, and reduced driving range [12]. As a by-product of the reactions inside the battery gas is generated, which is observed to sometimes being released when either stored or operated [9]. It is therefore important to better understand the behavior of Li-ion cells under different conditions as a way to improve their life-cycle rather than being forced to replace them, keeping costs down. [13]

## 1.1 Problem background

During normal cyclic operation, Li-ion cells tend to experience internal stress [13] due to swelling and contraction of the electrodes, *Solid electrolyte interface* (SEI) formation as well as gas and heat generation. Altogether, these effects will give rise to stress on the cell casing, causing an expansion and contraction of the cell. The formation of gas not only builds the pressure and causes the cell to expand, but it may also de-laminate the electrodes and de-contact the active material [14] leading to capacity loss [13] [15], aging of the cell and safety problems [14].

The rate of gas generation by chemical and electrochemical reactions inside the battery is dependent on the manufacturing quality, chemistry of the battery, type of cycling, and storage conditions of the battery [9]. Furthermore, ambient temperature, over-discharging, and charging also have an impact on the release of the gas [16].

Usually, the swelling is barely noticeable, but in some cases, particularly in pouch cells, it can be directly observed, see figure 1.2.

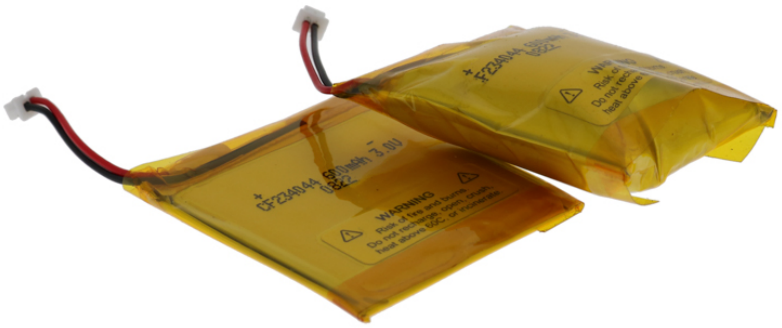

Figure 1.2: Comparison between a non-swollen pouch cell and a swollen pouch cell. [17]

Although the swelling effect in the single cell may be negligible, a more significant impact can result at the cell module level. The cells are packed very tight inside the module and thus have very limited space for expansion. Usually, when the battery enlargement is the multiple of its number of cells, the deformation or cracking of the module cover can be observed as in figure 1.3. The external pressure on a singular cell has also been found to influence the aging and capacity fading of the cell[18]. Hence this motivates research to study the swelling behavior in the beginning life of the battery pack from the cellular level, both because of module concerns and aging and capacity loss of the cell. Especially regarding the swelling behavior concerning temperature, c-rate, and *state of charge* (SOC).

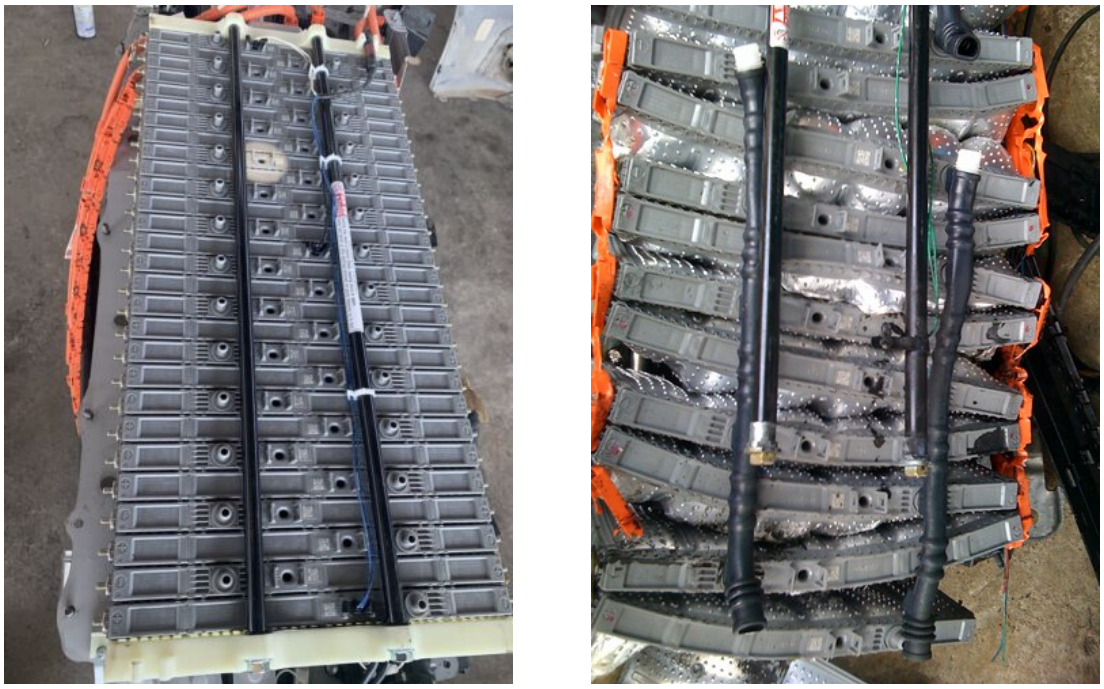

(a) New Toyota Prius battery module [19]

(b) Swollen Toyota Prius battery module [20]

Figure 1.3: Battery modules a.) not cracked and b.) cracked due to swelling

## 1.2 Purpose

The purpose of this thesis is thus to investigate and model the swelling behavior of a prismatic Li-ion-graphite/NMC-cell at the *Beginning of Life* (BoL).

## 1.3 Previous work

Oh, et al [1] studied the thickness change during one cycle in a prismatic graphite/NMC cell at different points, see figure 1.4. The thickness increase showed a maximum in the center of the cell (≈ 0.8 % expansion of initial thickness) (point 3 in figure 1.4) with much less significant expansion at the edges of the cell at about 0.3% (point 2 in figure 1.4). At a low c-rate where thermal swelling effects were deemed negligible, a maximum increase of 1.5% of initial thickness was observed, thought to mainly be attributed to the intercalation of Li-ions in the electrode materials.

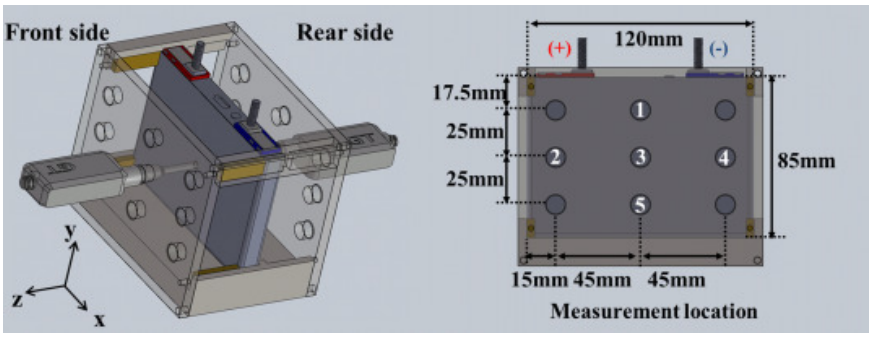


Figure 1.4: Schematic diagram of the experimental setup showing the fixture, the cell, and the thickness measured locations 1–5. [1]

During cell operations, there tends to be gas generation by unwanted side reactions[21] [22]. The rate of decomposition increases along the battery usage. Over-discharge and charge current also cause a spike in the $CO_2$ gas percentage inside the cell. These decomposed gases exert pressure on the battery case from the inside [13], [17]. The observation made by Seon-Hong and In-Hwan [22] while dissecting a cell post usage states that the gas was accumulated between the jelly roll layers and between the jelly roll layer and casing. Also, the anode surface had different color variations indicating most of the side reactions happened in the anode.

Studies have also shown that the thermal swelling of the cell is influenced by the c-rate. Oh, et al.[23] observed the thermal swelling of a Li-ion cell. They found a high dependency on c-rate as well as on SOC. Additionally, at high temperatures, the thermal swelling appeared linear, while at low temperatures the swelling was shown to be quadratic in nature.

Finally, when it comes to the modeling of pressure changes in Li-ion cells there have been some quite successful phenomenological swelling models such as those described by Oh, et al [24], and also full electrochemical multiscale models as described by Clerici, et al [25] which could capture the pressure changes in a prismatic Li-ion cell. Research students Gutpa [26] and Govindaraj [27] proposed a physics-based model that requires a large number of cell internal designs and kinetic parameters, which is a cumbersome process to extract. Additionally, cell suppliers sometimes restrict the possibility of opening up the cell to investigate it internally. The complexity of these models opens up the possibility of making a more simple model, without the need for extensive testing on or opening up the cell.

## 1.4 Ethical considerations in this work

Li-ion batteries are one of the most sustainable solutions when it comes to energy storage and propulsion of cars [28], since in the end product, there is almost no environmental impact of their usage aside from electricity production. However, one also has to take into consideration the mining of Li and other necessary raw materials as well as the transport of these and the production of the actual cell. Thus it is very important to optimize the use of Li-ion cells in order to increase their life span as much as possible. Through this thesis, more knowledge is given to how the development of pressure and stress inside the battery cell takes place. As higher external pressure on the cell casing has been linked to increased capacity fade, knowledge about how the pressure develops inside the cell at the beginning of life could allow us to increase the existing lifespan of the cell. This is very positive from a sustainability perspective as well as from an ethical viewpoint since fewer raw materials will have to be mined and thus also less chance for people to be exploited.

# Chapter 2

# Theory

In this chapter, relevant theory necessary for the analysis of the experiments and discussion of results is presented.

## 2.1 Overview of Lithium Ion Cells

A lithium-ion cell is an electrochemical cell that reversibly stores and shuttles Li-ions between the anode and cathode materials. It consists of five main parts, An ion-containing electrolyte, allowing ionic transport but being electronically insulating, a *separator* which blocks electron transfer but allows for ionic transport, an *anode* whereby an oxidizing reaction with the electrolyte produces electrons while discharging and ions, a *cathode* that accepts electrons due to a reducing reaction with the electrolyte while discharging, two current collectors that collect electrons from cathode and anode and finally an external electric circuit connecting the current collectors permitting electron flow between anode and cathode, see the schematic Fig 2.1. During charge, Li-ions as well as electrons flow from the cathode to the anode.

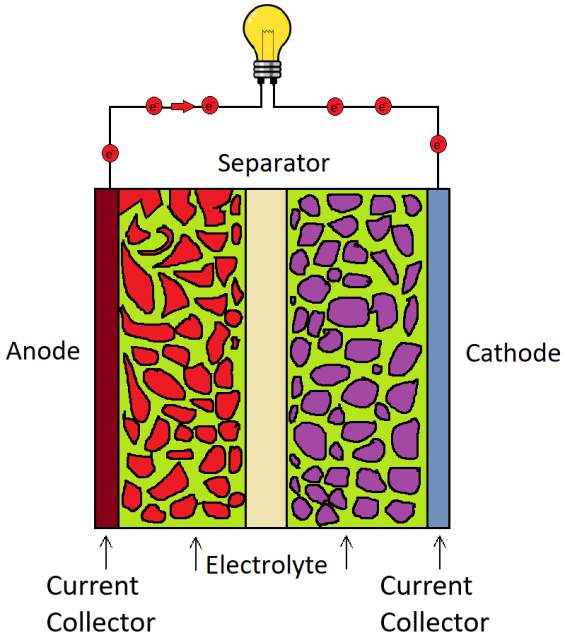


Figure 2.1: The four main parts of a lithium-ion cell: Anode, Cathode, Separator, Current collectors, and Electrolyte.

The *open-cell-voltage*, *OCV*, of the cell is the characteristic voltage of the cell without any

load and is defined as the difference in electrochemical potential between the anode and cathode [29],

$$OCV = \frac{\bar{\mu_c} - \bar{\mu_a}}{-e} \tag{2.1}$$

where $e = 1.602 \cdot 10^{-19} C$ is the electronic charge and $\bar{\mu_c}$ together with $\bar{\mu_a}$ are the electrochemical potentials of the cathode and anode respectively. Due to internal resistances, the measured voltage will be different from the OCV as,

$$V_{measured} = OCV - IR_i \tag{2.2}$$

where $I$ in (2.2) is the charge/discharge current, which is negative on discharge, and $R_i$ is the internal resistance of the cell. Thus (2.2) will yield a higher value than the $OCV$ on charge and vice-versa on discharge. (2.2)

### 2.1.1 Intercalation

The most common way of reversibly storing Li-ions in the electrodes is through a process known as *intercalation*. In essence, this means that the Li-ions are stored in available sites in the electrode structures. The process can be described as follows,

$$xLi(Anode) + \varepsilon Li(Cathode) \rightleftharpoons (x - y)Li(Anode) + (\varepsilon + y)Li(cathode) \tag{2.3}$$

where $x$ and $\varepsilon$ are the number of Li-ions in the anode as well as a cathode at full charge, and $y$ is the number of Li-ions that are removed from the anode material and added to the cathode material during full discharge. There is a non-zero amount of Li-ions, $\varepsilon$, in the cathode material at full charge since its structure becomes less stable if it is allowed to delithiate too much[30]. Note that left to right in (2.3) denotes discharge and right to left meaning charge.

A quite illustrative example of how the Li-ions are stored in an intercalation electrode material can be made with graphite, one of the most commonly used anode materials in Li-ion cells. It is made up of layers of carbon stacked vertically, each layer consisting of a hexagonal grid of carbon atoms, see figure 2.2.

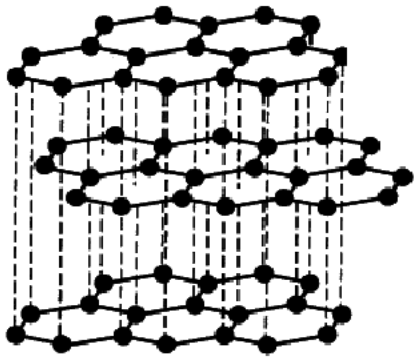

Figure 2.2: Multiple Layers stacked [31]

In the graphite lattice the available sites for the Li-ions occur in the center of these hexagons, see 2.3.

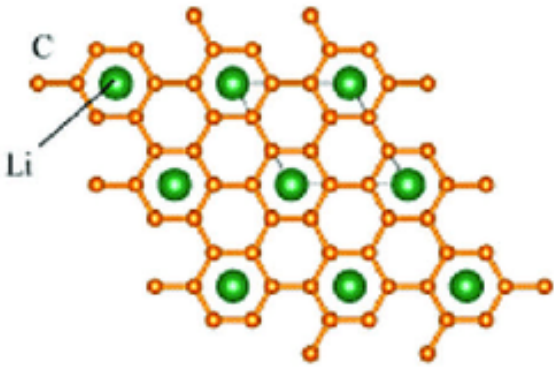


Figure 2.3: $LiC_6$ structure [32].

Fully *lithiated* graphite, meaning that Li-ions have filled all available lattice sites, therefore has 6 carbon atoms per 1 Li-ion, thus having the chemical formula $LiC_6$.

In reality, the electrode structure will change in order to accommodate the Li-ions, leading to slightly different material properties depending on the *degree of Lithiation* and also the expansion and contraction of the electrodes.[33][34] [35]

### 2.1.2 Electrode Materials

As previously mentioned, graphite is usually used for anode material, and has a theoretically fully lithiated specific gravimetric capacity of 372 $mAhg^{-1}$[36]. The cathode material is often a *transition-metal oxide*, such as *Li-Ni-Mn-oxide* (NMC) most commonly $LiNi_{0.33}Co_{0.33}Mn_{0.33}O_2$, *Lithium nickel oxide* (LNO), $LiNiO_2$, and *Li-Mn-oxide* (LMO), $LiMnO_2$, with specific capacities of 280mAhg$^{-1}$ [37], 225mAhg$^{-1}$, and 120mAhg$^{-1}$ respectively[38]. Each offers both advantages and disadvantages, and their usage depends on the application, see figure 2.4.

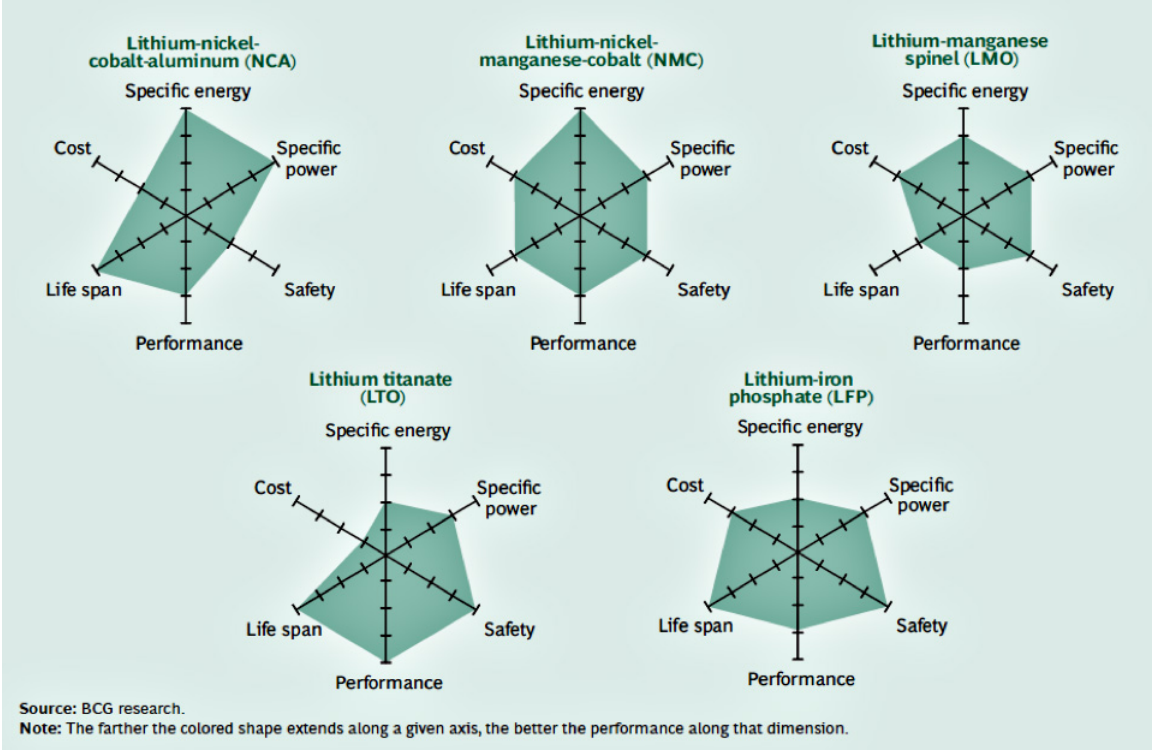


Figure 2.4: The advantages and disadvantages of different lithium-ion battery cathode materials from [39].

### 2.1.3 Electrolyte

The operating voltage window decides which electrolytes can be used in the cell. The electrolyte is selected so that the electrochemical potentials of the anode and cathode are not too far off from the *Highest Occupied Molecular Orbital* (HOMO) and *Lowest Occupied Molecular Orbital* (LUMO) of the electrolyte. That is,

$$OCV = \bar{\mu_A} - \bar{\mu_c} \leq E_g \tag{2.4}$$

where $E_g$ is the energy difference between the HOMO and LUMO energy levels. If $\bar{\mu_A} > HOMO$ the electrolyte may be reduced on the anode forming a *Solid Electrolyte Interface* (SEI). Additionally, if $\bar{\mu_C} < LUMO$ the electrolyte will be oxidized on the cathode. For Li-ion cells, the voltage window is often $> 4V$ and as such, aqueous electrolytes with $E_g \approx 1.3eV$ is not applicable. Instead, non-aqueous electrolytes are used.

In the case of a graphite/NMC cell, the $OCV$ at 100 % is about 4.2V[40]. This means that aqueous electrolytes with $E_g \approx 1.3eV$ cannot be used and thus Li-ion cells usually contain non-aqueous electrolytes with much wider electrochemical windows such as organic and polymer electrolytes[41]. The redox formation energy of graphite also lies above the HOMO of the most commonly used electrolytes and as such SEI will always be formed on a graphite anode. Additionally, SEI formation also causes increased internal resistance of the cell[33].

## 2.2 Volume changes in Li-ion cells

There are several ways whereby volume change can occur in Li-ion cells, both reversible due to heating as well as intercalation, and irreversible due to *solid electrolyte interface* (SEI) as well as gas formation. While cycling, the non-uniform intercalation of the Li-ions in the electrode materials will cause mechanical stress within the active materials [42]

### 2.2.1 SEI formation

The SEI layer is mostly found on the surface of the graphite particles as in figure 2.5. It forms initially in the cell's formation cycle and increases in thickness as the cell ages. The SEI formation on the electrodes will cause an irreversible volume increase in the cell. The thickness and composition of the SEI layer will depend on the electrode materials as well as the electrolyte but it is generally 10-100 nm thick[43].

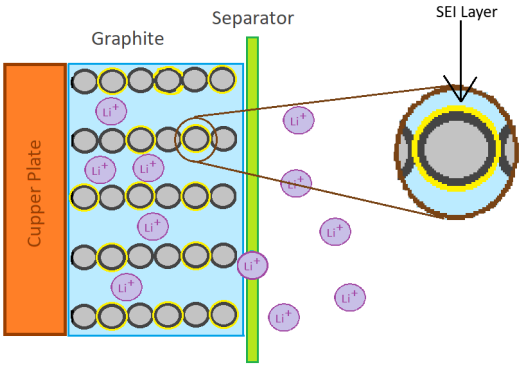


Figure 2.5: Formation of the SEI layer.

### 2.2.2 Intercalation related effects

When lithium ions are intercalated into the anode and cathode materials, the crystal structures will change in order to accommodate them, and the unit cell volume will change accordingly. During charging, a graphite anode can expand from 10[44] up to 13.2%[45] while an NMC cathode decreases in unit cell volume from 2 to 8% depending on NMC type[46][47]. Overall this causes a net expansion of the cell and vice versa while discharging the cell.

### 2.2.3 Thermal expansion

Heating in a Li-ion cell comes from a number of sources, both when the cell is charged/discharged and initially when the current is switched off. The internal resistance in the cell generates what is known as *ohmic heating* and is irreversible since there is no similar reverse process. Additionally, there is reversible *entropic heating*, heating from electrochemical and other chemical reactions in the cell, and lastly heat of mixing due to the formation and relaxation of concentration gradients. [48] Overall the heat balance can be written as follows,

$$\dot{Q} = \left(IV - \sum_l I_l U_l^{avg}\right) + \sum_l I_l T \frac{\partial U_l^{avg}}{\partial T} + c_p \frac{dT}{dt} + \sum_k \Delta H_k^{avg} r_k + \int \sum_{ij} (\bar{H}_{ij} - \bar{H}_{ij}^{avg}) \frac{dc_{ij}}{dt} dv \quad (2.5)$$

where $I$ is the current, $V$ is the cell potential, $I_l$ is the current for electrochemical reaction l, $U_l^{avg}$ is the volume averaged open circuit potential for electrochemical reaction $l$, $T$ is the temperature, $C_p$ is the specific heat capacity, $\Delta H_k^{avg}$ is the volume averaged enthalpy change for a chemical reaction $k$, and $\bar{H}_{ij}^{avg}$ is the volume averaged partial molar enthalpy of species i in phase j, and lastly $c_{ij}$ is the concentration of species i in phase j. The first term in (2.5) describes the irreversible ohmic heat, the second is the reversible entropic heat, the fourth is heat generation due to chemical reactions in the cell and the last is the heat generated due to the creation of concentration gradients and subsequent relaxation of them. Omitting the heat of mixing it is possible to write the heat balance in the following, simpler way,

$$\dot{Q} = I(V - U) + IT \frac{\partial U}{\partial T} \quad (2.6)$$

where the first term in (2.6) is the irreversible ohmic heating and the second term is the reversible entropic heating.

Usually, the irreversible entropic heat generation dominates and as such at high c-rates there will be considerable heating in the cell[49][50]. When the current is turned off the heating of mixing described in (2.5) will come into play and will cause further heating of the cell[48]. All these heating effects will cause volume expansion.

## 2.3 Types of Lithium-ion cells

A Li-ion cell can be classified based on different cell designs, materials used, and applications. For vehicle applications, there are three kinds of cell designs used namely: cylindrical, pouch, and prismatic[50]. They differ essentially in the way they are packed, but all have the same component parts of alternating cathodes, separators, anodes, and current collectors but are folded in different ways. The anode current collectors are often aluminum and the cathode ones are often made of copper[51]. Each different cell design has its drawbacks and advantages.

### 2.3.1 Cylindrical cell

In the cylindrical cell, the sheets of the anode, separator, and cathode are rolled as a jelly roll as shown in figure 2.6b to a certain diameter as per requirement 2.6a. This determines the energy storage ability of the cell. The manufacturing of the cell is not complex but the thermal control is difficult. They also consume additional space while packaging creating voids between the cells. Regardless, those spaces can be used to run the coolant pipes for better temperature regulations[52].

(a) Some kinds of the cells available in the market [53].

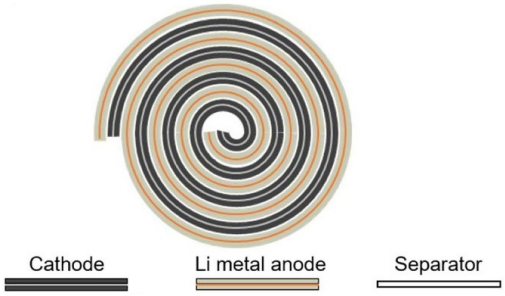


(b) Cylindrical cell windings[54].

Figure 2.6: Cylindrical cells

### 2.3.2 Pouch cell

In a pouch cell 2.7b, the electrode sheets are instead either stacked on each other or folded in a Z-like form [52] as seen in figure 2.7a.

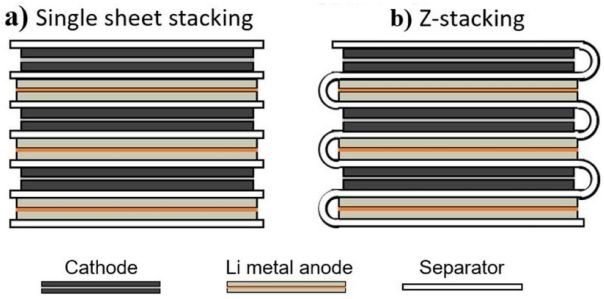


(a) Different types of Pouch cell structures[54].

(b) Cells available in the market[55].

Figure 2.7: Pouch cells

### 2.3.3 Prismatic cell

Lastly, in the prismatic cell, the electrode sheets are also rolled, but in a different way from cylindrical cells, as shown in figure 2.8a and 2.8b. Sometimes Z-folded prismatic cells can also be found [52]. The winding is covered with a hard casing material such as aluminum or reinforced plastic. These kinds of cells have excellent packaging efficiency. The temperature difference between the cells is uniform while the reduction of heat in the cell module is always a challenge[52].

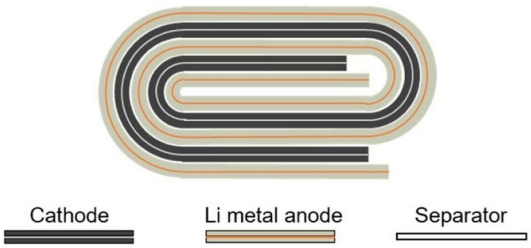


(a) Structure of Prismatic cell [54].

(b) Cells available in the market [56].

Figure 2.8: Prismatic cells.

# Chapter 3

# Methods

In this section, the performed experiments and subsequent modeling are described. The cycling tests were designed based on the cell specifications, and the test-rig was studied before starting the experiments. The data obtained from the experiments was analyzed in *Matlab* [57] and *Python*. The model was run in *COMSOL Multiphysics*[58].

## 3.1 Experimental set-up

### 3.1.1 Cell specifications

A prismatic cell with Graphite/NMC electrodes was used. Its operating range is 2.8 to 4.2 volts and has a nominal capacity of 50 Ah. The cell was at the beginning of its life with the completion of its formation cycles.

### 3.1.2 Test Protocol

In order to study the overall behavior of the pressure during full cell charge and discharge the pressure change was measured for several c-rates over the entire SOC range, see table 3.1.

Table 3.1: C-rates used for normal cycling

| C-rate | Current (A) |
|---|---|
| 0.1 C | 5 |
| 0.2 C | 10 |
| 0.3 C | 15 |
| 0.5 C | 25 |
| 0.8 C | 40 |
| 1 C | 50 |
| 1.2 C | 60 |

At the start of each cycling test, the cell was first completely discharged in order to test it for the full capacity range. This was followed by two hours of rest allowing the cell to relax. In order to have as comparable data as possible, three full cycles were subsequently performed for each C-rate as shown in figure 3.1. Each charge and discharge was followed by two hours of rest in order to relax the cell. The first cycle was only used in order to ensure that the cell was in a similar state for all experiments and was later discarded, with only the 2 latter cycles being kept for analysis.

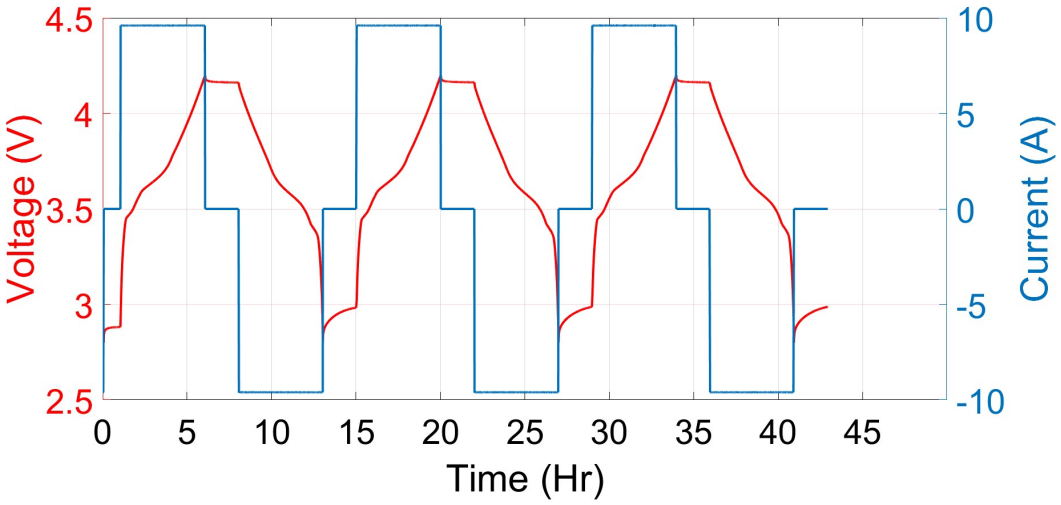


Figure 3.1: Current input and voltage response for 0.2 C.

### 3.1.3 SOC estimation

The SOC of the cell is calculated from the input current applied to the cell by coulomb counting, where the initial voltage after initial relaxation during the charge is considered as 0% SOC and it is assumed that the cell reaches 100% SOC the instant it has reached 4.2 $V$. Similarly on discharge, 100% SOC is assumed to be the relaxed voltage when the discharge starts and is assumed that 0% SOC has been reached when the voltage reaches 2.8 $V$.

### 3.1.4 Test-Rig

The scope of the thesis was to use an already existing test-rig to conduct experiments and develop a model rather than to develop a test-rig. Therefore, a pre-existing test rig from [59], made for pouch cells was used.

The test jig is described below in figure 3.4a. It is made up of 3 aluminum plates held together vertically by 4 long screws at the corners. 4 load cells sit equally spaced from the corners on the 24 *mm* thick bottom plate. The Li-ion cell then fits on the 24 *mm* thick middle plate. Finally, a thinner, 13 *mm* thick plate, is fitted on top of the cell. In order to limit the possibility of short-circuiting the cell, the plate above and below the cell was covered with insulating tape.

An external force of 2000 $N$ (i.e. 148.5 $kPa$) is exerted on the cell by fastening the nuts on the bolts to mimic the force applied on the cell when they are assembled in the module[18]. The cell was connected to a *Maccor series 4000* cell cycler whereas the load cells were connected to the CAN bus of an IPETRONIK MSENS-2 device.

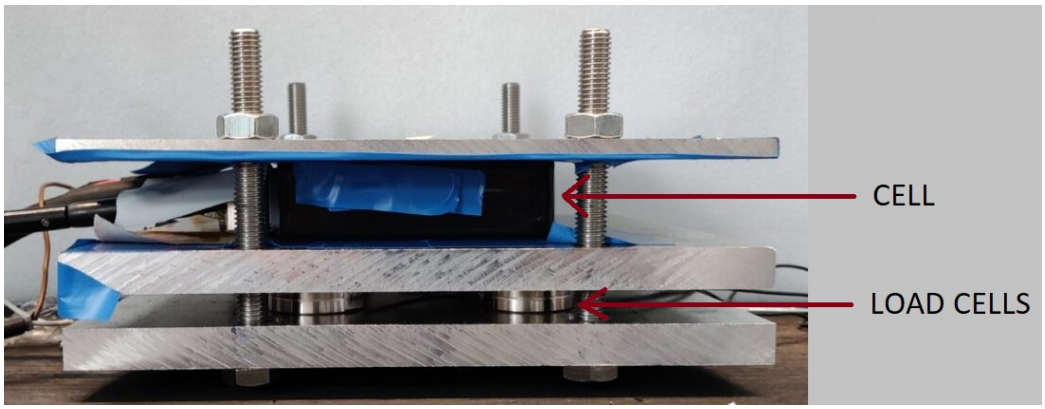


Figure 3.2: The test-rig used for the experiment from [59].

### 3.1.5 Load sensors

**F23 load cells**

The load sensors used were *FC23 compression load cells*[60], as shown in figure 3.3a. A total of four load sensors were used and their positions on the plate are illustrated in figure 3.3b. Each sensor is capable of measuring forces between 0 to 4.454 $kN$ (307 $kPa$). It uses a supply voltage of 5V and has a non-zero force output of $\pm 20mV$ [60]. The load sensors were calibrated with an LCB compression load cell [61] which can measure forces from 0 $N$ up to 20 $kN$ (1379 $kPa$).

During initial experiments, it was observed that the measured force was not even throughout the plate, assumed to be due to a see-saw effect due to the fact that the plate was not perfectly horizontal. As an effect there was a substantial difference in the force measured by the different load sensors. Thus only data from sensor number 1, seen in figure 3.3b was used for analysis.

(a) A Single FC23 compression load cell.

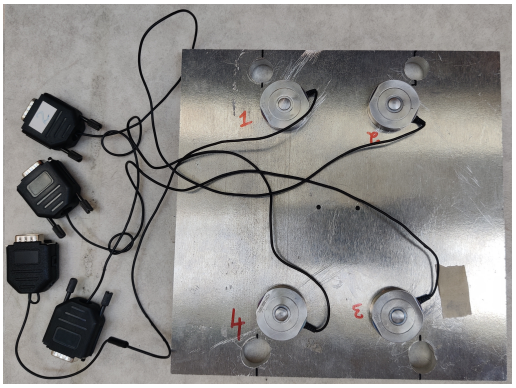

(b) The placement of the four Load cells in the test-rig.

Figure 3.3

### 3.1.6 M-SENS2

The M-SENS2 is an IPETRONIK unit that allows analog data from a sensor to be sent through a CAN bus to a computer. It has 4 analog input channels, with a channel sampling rate from 1 $Hz$ up to 2000 $Hz$. Additionally, any voltage required for the sensors can go through these input channels [62]. It has a DC voltage requirement of 12V up to 35V,

powered by an external DC source with an adjustable voltage supply, see figure 3.4b. The total voltage requirement was calculated from the voltage requirement of load sensors [60] and the IPETRONIK [62] unit. The sampling rate for the pressure sensor used was 1 $Hz$.


(a) M-SENS2 analog input module.

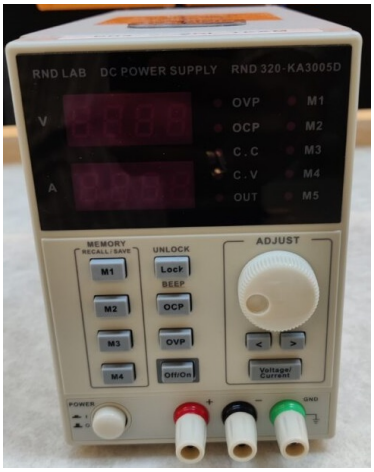


(b) The DC Source used.

Figure 3.4

### 3.1.7 Cell Cycler

The cell was cycled using a *Maccor series 4000*[63] cell cycler that can handle currents from -120A to 120A and voltages ranging from 0 to 5V. The test protocols are designed in the *Build Test* software integrated with Maccor. The cell cycler then follows these commands and runs the test on the cell accordingly.

## 3.2 Modelling

The pressure change was modeled as the circuit in figure 3.5 with an equivalent equation 3.1, assuming that the pressure response of the cell is analogous to the voltage response of a battery with internal resistance.

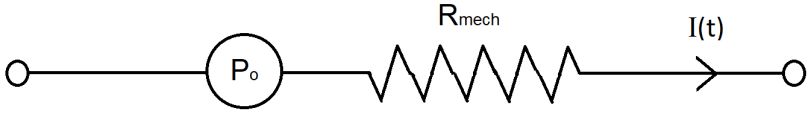


Figure 3.5: Equivalent Circuit Diagram for the model.

The pressure response can also be assumed to be SOC dependent, and can thus be written in the following way,

$$P_{cell}(SOC(t), T(t), I(t)) = P_o(SOC(t), T(t)) + \mathfrak{R}_{mech}(SOC(t), T(t), I(t)) \cdot I(t) \tag{3.1}$$

where $P_{cell}$ is the resulting cell pressure and $P_o$ is the relaxed pressure at a particular SOC and temperature both with unit pascal. $\mathfrak{R}_{mech}$ is the expansion resistance of the cell, the mechanical resistance of the cell to resist expansion with the unit (pascal/ampere). Note that the cell pressure depends on the SOC, temperature as well as the current.

The expansion resistance in (3.1) for a given c-rate x was calculated in the following way,

$$\mathfrak{R}_{mech,x} = \frac{P_x - P_{0.05}}{I_x} \tag{3.2}$$

where $P_{0.05}$ is the Pressure response for the lowest experimental c-rate, 0.05c, and $P_x$ as well as $I_x$ is the Pressure response and the absolute value of the experimental current at c-rate x respectively. An illustrative figure can be seen below with the 0.5C charge pressure experiment as an example.

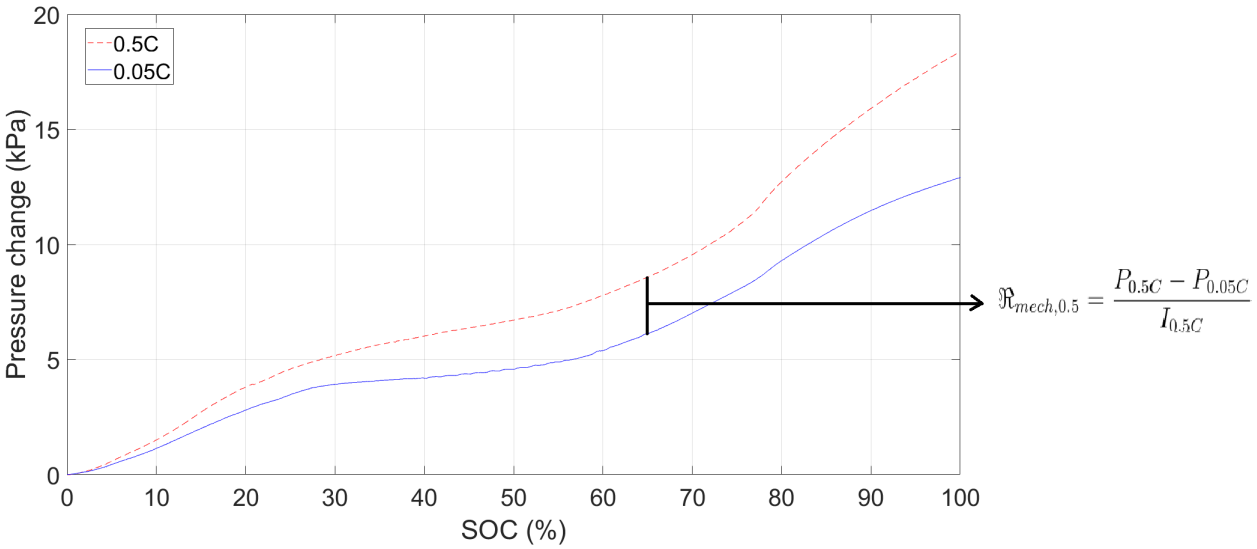


Figure 3.6: Illustration showing how the $\mathfrak{R}_{mech}$ values were obtained.

Due to time limitations, the modeling was only done for the charging case. A lookup table with $\mathfrak{R}$ values was created using pressure data from 0.1C, 0.2C, and 0.5C. These resistance values were then interpolated to each desired c-rate and the pressure response could be calculated as described in (3.1). Higher c-rates than 0.5C was not used due to bad data. The model was subsequently validated with data from [1] and [2] taken with the use of *WebPlotDigitizer*[64].

# Chapter 4

# Analysis

In this section, the results, analysis as well as discussion of results, are presented. Analysis of the gathered experimental data was done with *Python* and *Matlab*. Validation data, using the results from two research articles, [1] and [2], is also presented.

## 4.1 Experimental observations

The pressure change over time is observed for one 0.2C in figure 4.1. The data shows that the pressure change in the cell is reversible, with the cell expanding while charging and contracting while discharging, due to intercalation and de-intercalation of Li-ions. The intensity of the pressure developed will depend on the electrode composition, cathode material, electrode balancing, and so on [2].

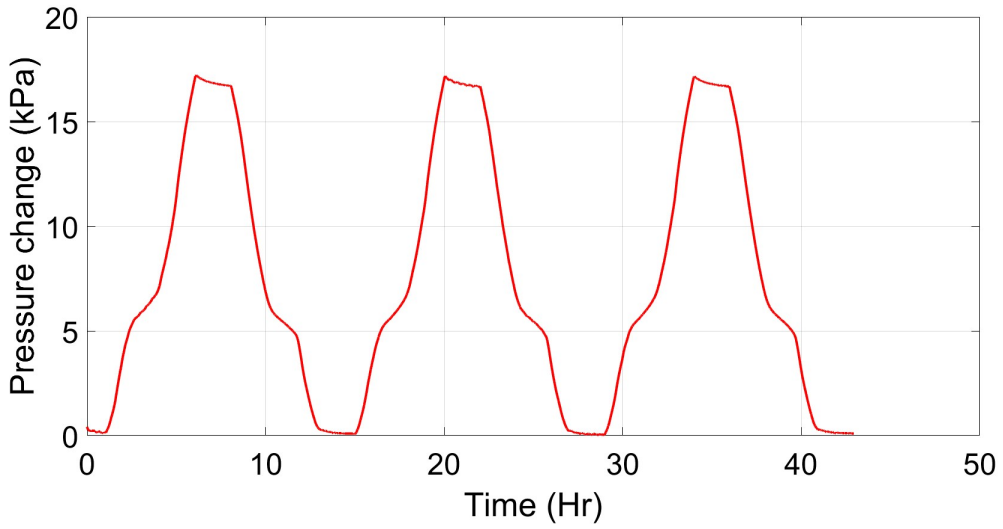


Figure 4.1: Pressure response for the c-rate 0.2C.

It can also be observed that the charge and discharge are not symmetric with respect to each other, where the discharge curve is lower at a similar SOC compared to the charging case. This might be due to some memory effect, where the cell has not had time to mechanically relax when the discharge starts. Also, it could be due to the fact that the voltage at discharge is always lower than the voltage at charge. This effect could be translated to the pressure that is exerted on the cell casing.

The charge pressure measurements for the c-rates from 0.1C to 0.5C are displayed in figures 4.2 and 4.3 below for charge and discharge respectively.

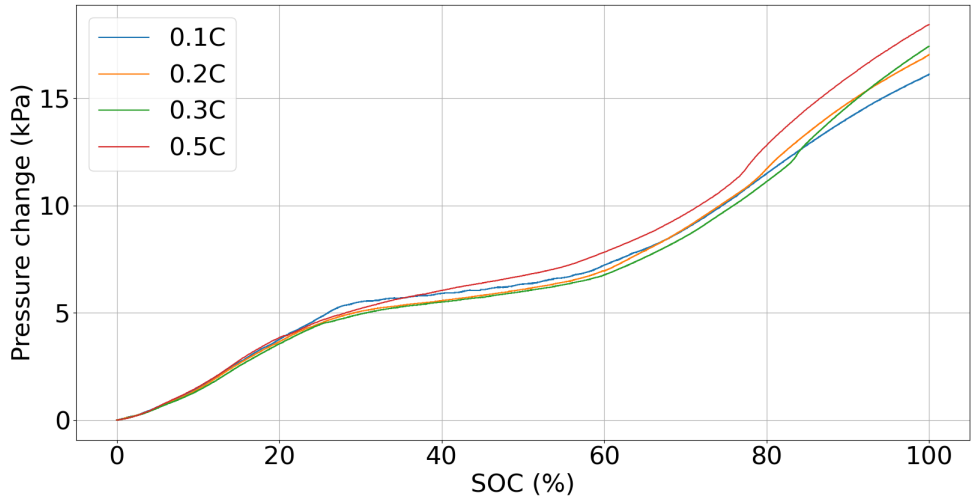


Figure 4.2: Pressure response over SOC for charging at c-rates from 0.1C to 0.5C.

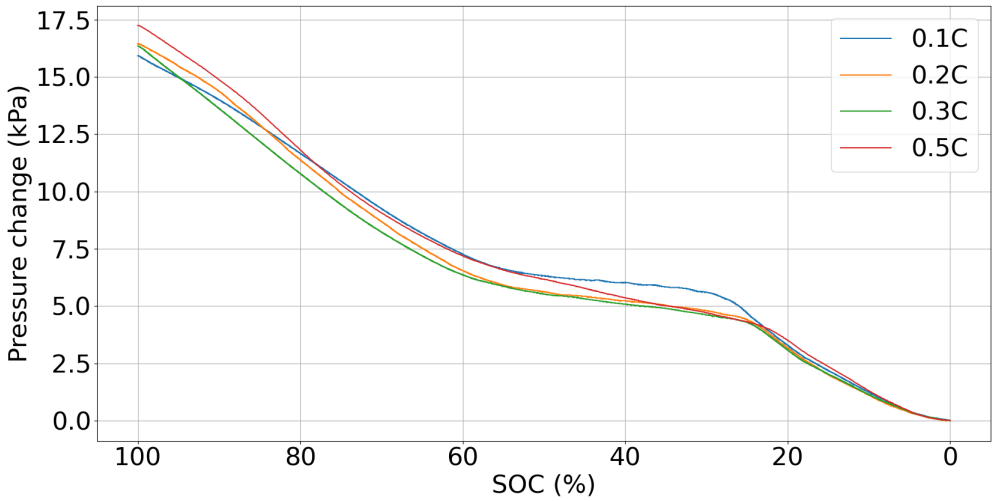


Figure 4.3: Pressure response over SOC for discharging at c-rates from 0.1C to 0.5C.

There seem to be some trends in the data. For low c-rates, up to 0.5C, as the c-rate increases, so does also the pressure change for both charge and discharge. This is reasonable since faster intercalation of Li-ions into the electrodes should provide more strain on the cell and thereby more expansion. At low c-rates, the swelling due to any thermal effect is less, as heat generated in the cell is comparatively low.

Instead now looking at the pressure change for charge and discharge from 0.5C and up to 1.2C in figures 4.4 and 4.5 there is a different trend. The maximum pressure change goes down with increasing c-rate. This is contrary to what one believes should happen. With increasing c-rate the mechanical stress increases due to non-uniform intercalation and diffusion-limited stress within the electrode materials and thus more expansion of the cell casing is expected. Additionally, the cell will probably start to experience some heating effects at higher c-rates, causing it to expand even more. At c-rates above 0.5 to 1.2, the maximum pressure change at 100% SOC instead decreases for increasing c-rates. The reason for this behavior could lie in the setup of the test-rig used in the experiments. From

previous studies [1] it has been shown that the swelling in a prismatic cell happens mainly in the center of the casing. However our test-rig had the load sensors in the corners, see figure 3.3b in Methods. Thus when the swelling becomes too big, the test-rig might have difficulty capturing it correctly, and instead, lower pressures than the actual pressure are observed since the cell does not swell as much at the edges. It could be that 0.5C is the limit for the current set-up and in order to get good data for higher c-rates the test-rig has to be changed, for example by placing a load sensor below the center of the cell. Another reason for the trend at higher c-rate could be that the test-rig for higher pressures acts as a spring and absorb some of the force leading to lower force measurement than what is actually exerted on the cell's surroundings. Additionally, it might be an effect due to the orientation of the set-up. As discussed in Methods 3 the experimental data showed a lot of variance between all load sensors due to the fact that the test-rig was not perfectly horizontal. At higher c-rates the expansion of the cell casing is more substantial than at low c-rates, which explains why more influence would be observed on the measurements.

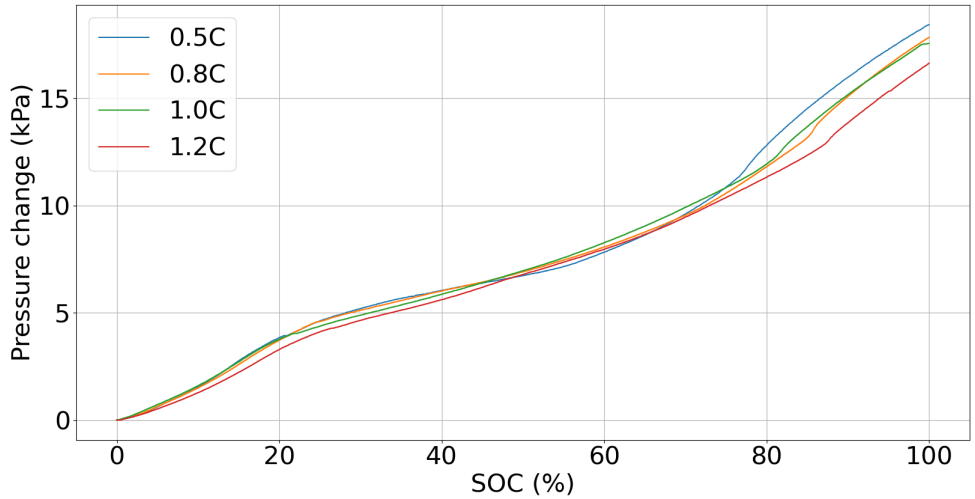


Figure 4.4: Pressure response over SOC for charging at c-rates from 0.5C to 1.2C.

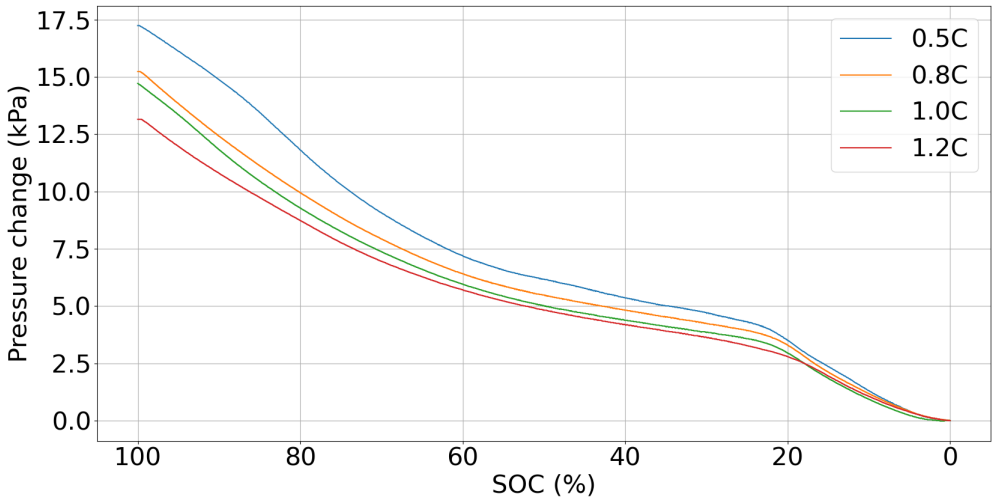


Figure 4.5: Pressure response over SOC for discharging at c-rates from 0.5C to 1.2C.

Below in figures 4.6, 4.7, 4.8 and 4.9 the Pressure and Voltage derivatives with respect to the SOC is displayed from C-rates at charge ranging from 0.1C to 1.2C. The corresponding derivatives for discharge follow the same trends as the charge derivatives and can be found in Appendix A.

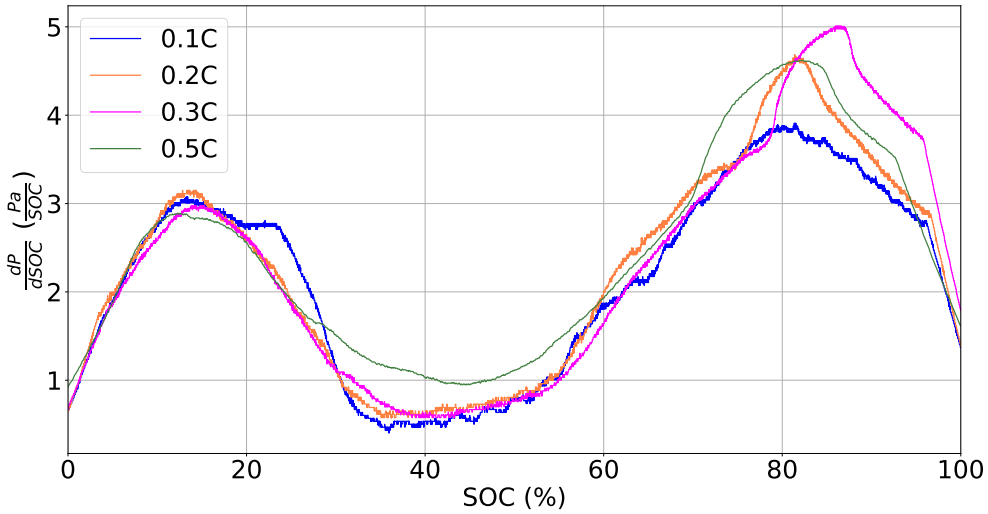


Figure 4.6: The Pressure derivative with respect to SOC for charging at c-rates from 0.1C to 0.5C.

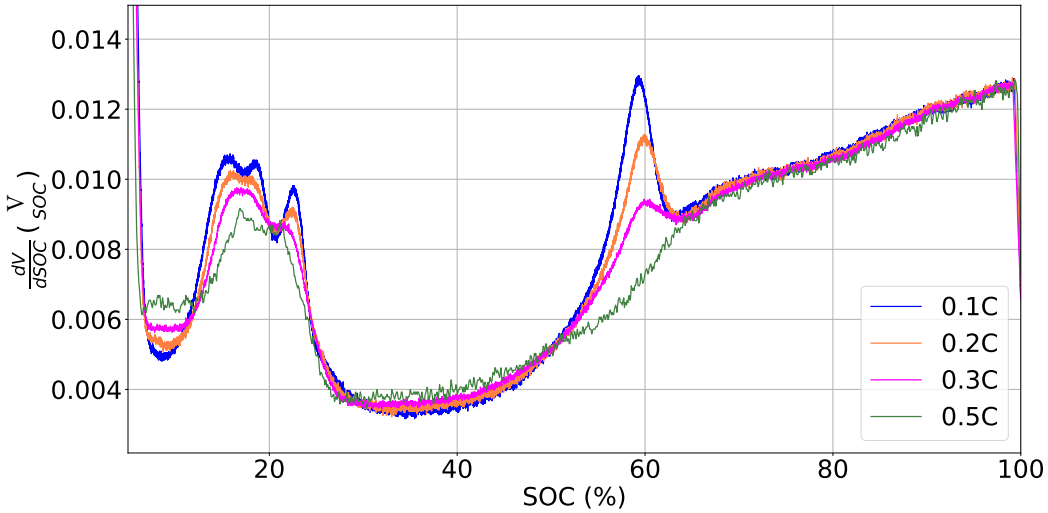


Figure 4.7: The voltage derivative with respect to SOC for charging at c-rates from 0.1C to 0.5C.

Looking at the c-rates from 0.1C to 0.5C in figures 4.6 and 4.7 the pressure derivative has two clear peaks for all c-rates at around 18% SOC and another at about 80 to 90% SOC. Meanwhile, the voltage derivative at the same c-rates also exhibits two peaks, one with a center at around 18% SOC and another at around 60 % SOC for all but 0.5C. There is also a curious relationship for 0.1C at the first peak for both pressure and voltage derivatives, where a first peak is closely followed by a smaller second peak, evident in both 4.6 and 4.7. The existence of peaks at similar places indicates that similar processes that control the voltage change in the cell also impact the pressure change. It is known that lithium intercalation into graphite does not happen instantaneously and instead happens in stages[65]. The first of

these stages, corresponding to a change to $Li_{0.2}C_6$ will happen at around 20% SOC which is exactly what is seen in figures 4.6 and 4.7. Another phase transition happens at around 60% SOC. Which is only apparent in the voltage derivative. The absence of this peak from the pressure derivative might however be due to a delay between the the phase transformation and the mechanical response at higher SOC. The peaks in the pressure derivative are also quite broad which could indicate that the pressure change is not as instantaneous as the voltage change and exhibits substantial lag-time. Similar behaviors can be seen for the pressure and voltage derivatives at higher c-rates in figures 4.8 and 4.9. Two peaks are observed for the pressure derivative but only one for the voltage. This could indicate that the phase transitions happen very fast at a higher c-rate and that there is not enough time for the behavior to be captured.

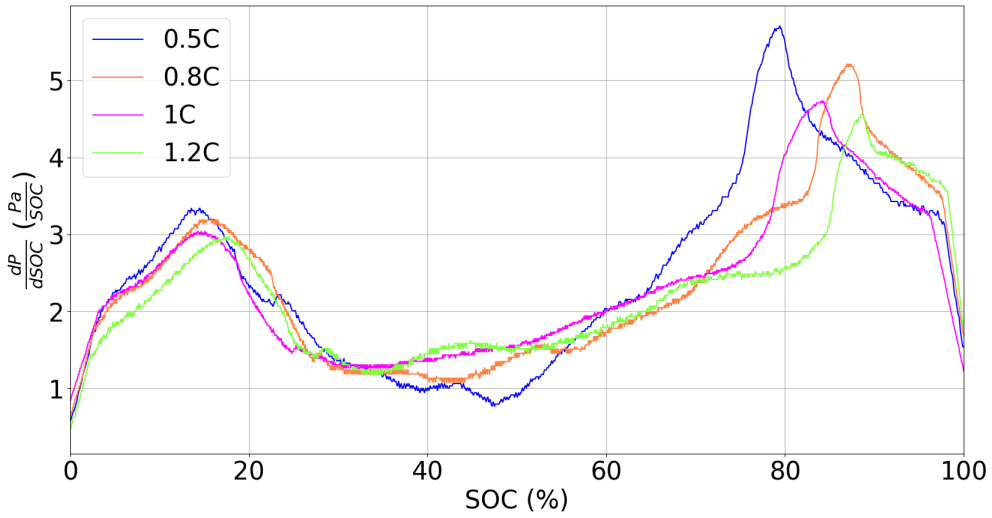


Figure 4.8: The pressure derivative with respect to SOC for charging at c-rates from 0.5C to 1.2C.

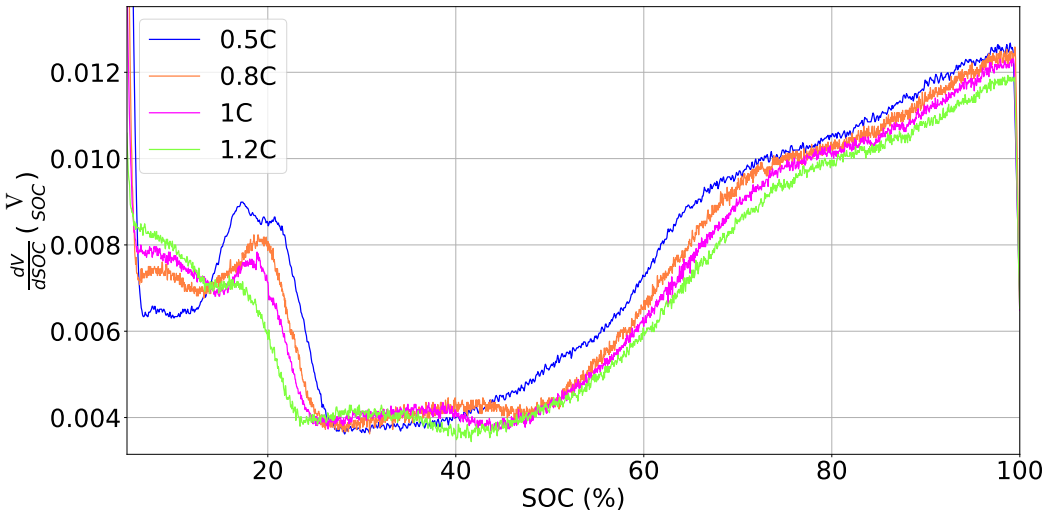


Figure 4.9: The voltage derivative with respect to SOC for charging at c-rates from 0.5C to 1.2C.

Figure 4.10 shows the behavior of both voltage and the pressure output from the cell for 0.2 C while second cycle charging and discharging. The pressure rises up to 1.4 to 1.5 times

the initial external pressure. The pressure increases sharply at the beginning of charging followed by a slow rate of expansion. After around 60% of charge the pressure inside the cell spikes. The same trend is noticed in the voltage response of the cell, so it can probably be attributed to a change in the state of the graphite to $LiC_6$. Similarly, during discharge, the cell pressure change also seems similar to the voltage response. From 0% DOD to 50% DOD, there is a drastic dip in the probably corresponding to a lithium-graphite phase transformation.[66]

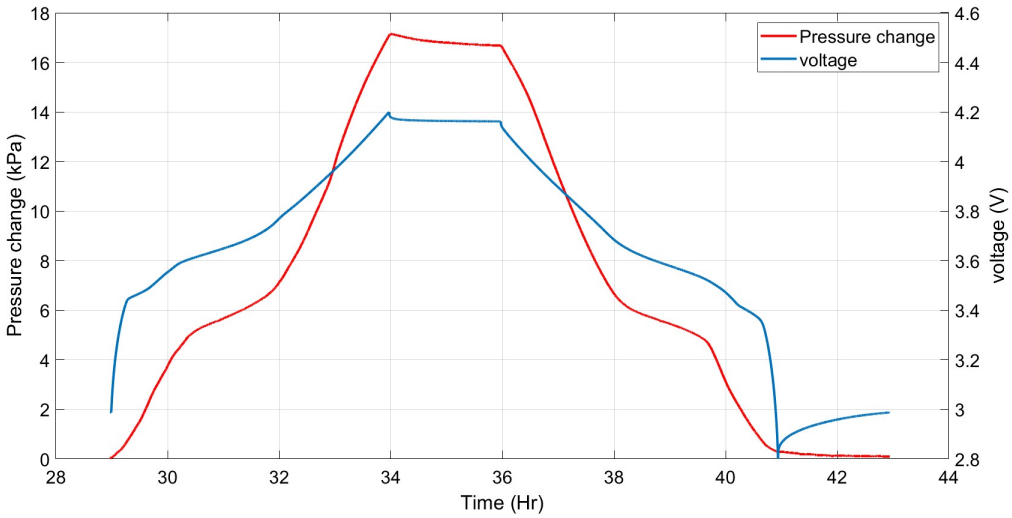


Figure 4.10: Pressure response and voltage over time for 0.2C.

## 4.2 Circuit modelling

The model pressure responses for three different C-rates were plotted together with experimental results, see figures 4.11a, 4.11b, 4.12a, and 4.12b below.

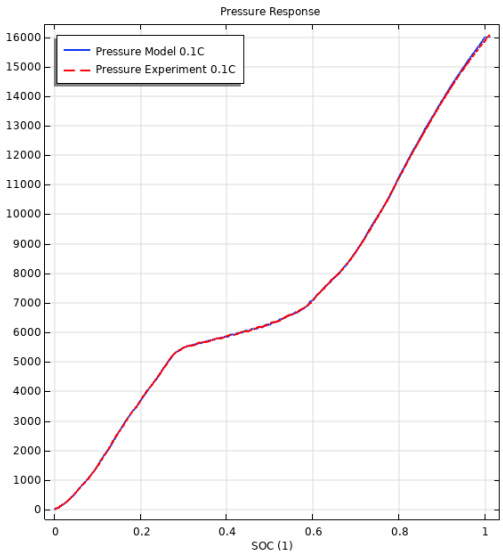


(a) Experimental pressure data comparison with the model for 0.1C.

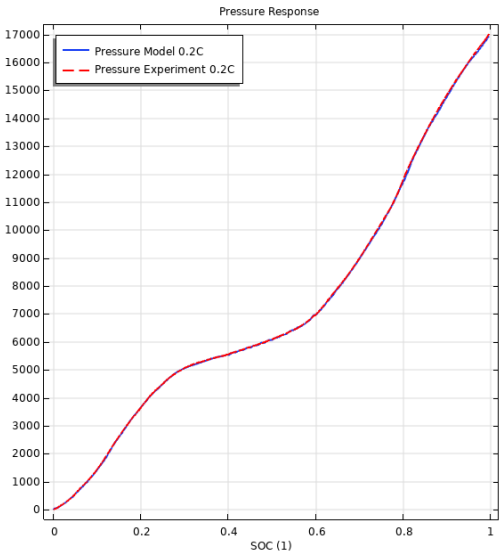


(b) Experimental pressure data comparison with the model for 0.2C.

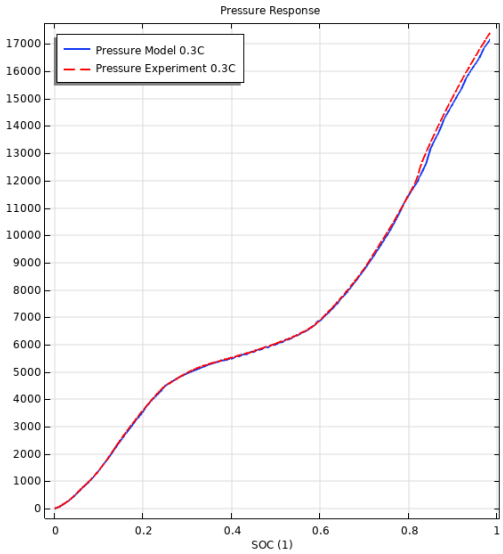


(a) Experimental pressure data comparison with the model for 0.3C.

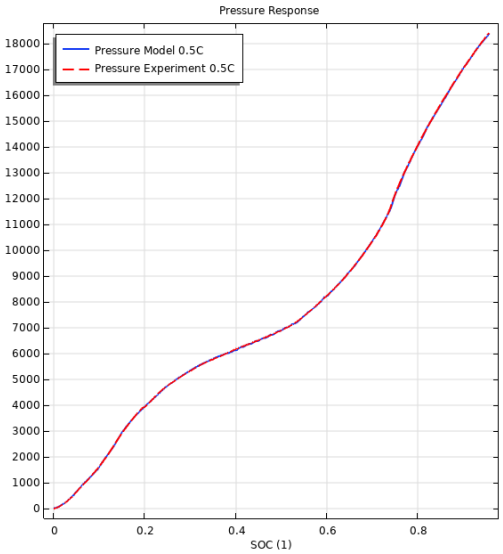


(b) Experimental pressure data comparison with the model for 0.5C.

Figure 4.12

Note that the model was created using data from 0.1C, 0.2C, and 0.5C, and therefore no error is expected between model and experimental data. For 0.3C (4.12a)the only C-rate where interpolation of the $\mathfrak{R}$-values was used shows quite a good fit, with an absolute error being presented in figure 4.13 below. As can be seen, the error is quite small quickly going to less than 1% absolute error between the simulated and experimental pressure response for 0.3C.

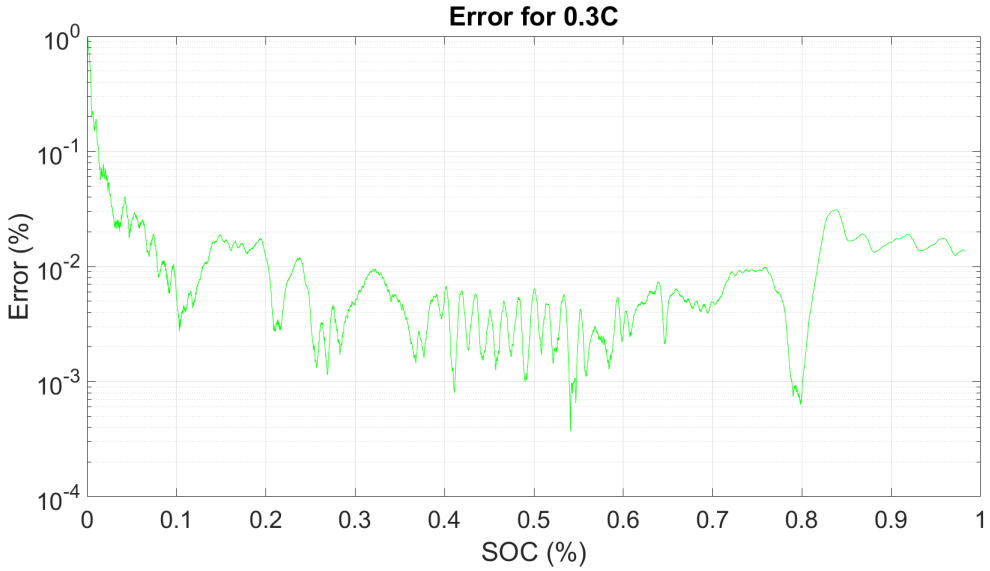


Figure 4.13: Absolute error between model and experimental results for 0.3C.

Lastly, the Resistance values for the different C-rates are displayed below in figure 4.14. There seems to exist quite a clear trend in the data, with higher resistance seen at a higher C-rate. This indicates that the used method is plausible, and shows the resistance to expansion increase at lower C-rates indicates that the cell is expanding less at lower C-rates.

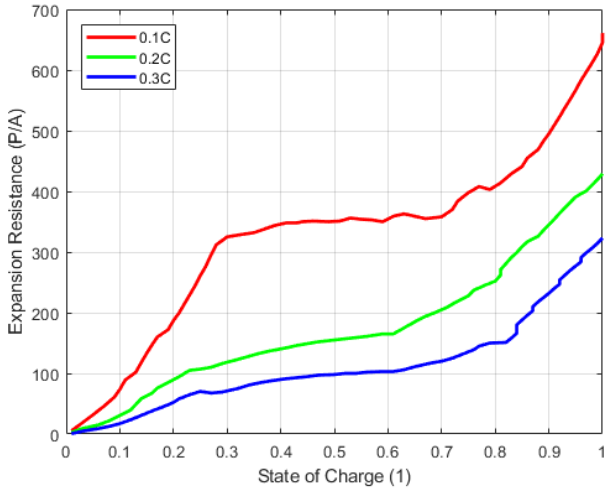


Figure 4.14: Comparison expansion resistance $\mathfrak{R}$ of different c-rates.

## 4.3 Validation

The model was validated by using data from two research articles, [1] and [2]. The validation is essential as it measures the confidence in the model. The expansion resistance $\mathfrak{R}$ was calculated for a number of c-rates in the particular paper as described previously, and the pressure response could then be calculated.

### 4.3.1 Paper 1: Rate dependence of swelling in lithium-ion cells

This study did similar experiments on a prismatic graphite/NMC cell and the authors proposed that the swelling is dependent on the c-rate of charging and discharging, thermal expansion, and phase transition [1]. Experimental data together with modeled data from the paper is depicted in 4.15a, 4.15b and 4.16a. These c-rates were also used for the $\mathfrak{R}$-values and as such the error between the model and experiment is zero. Note however that the c-rates used are higher than the c-rates used in this thesis and as such any conclusions from this validation should be drawn carefully. It seems however that the modeling method seems to work for this validation data, strengthening the hypothesis that the model actually works.

The calculated $\mathfrak{R}$ is also shown in figure 4.16b. They seem to have a different trend than the Resistance values calculated from data in this thesis, but this could be due to the higher c-rate used and should not be taken into too much consideration. Potentially it could be due to thermal expansion, which will play a much higher role at c-rates above 1C. However, all obtained resistance values exhibit a similar trend with on average decreasing resistances with increasing c-rate.

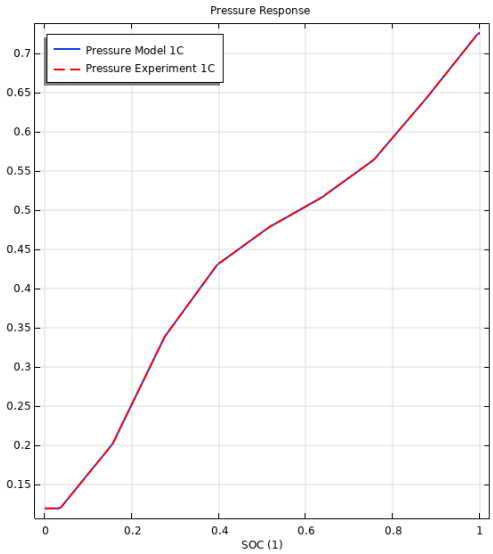


(a) Pressure data comparison with the model for 1C.

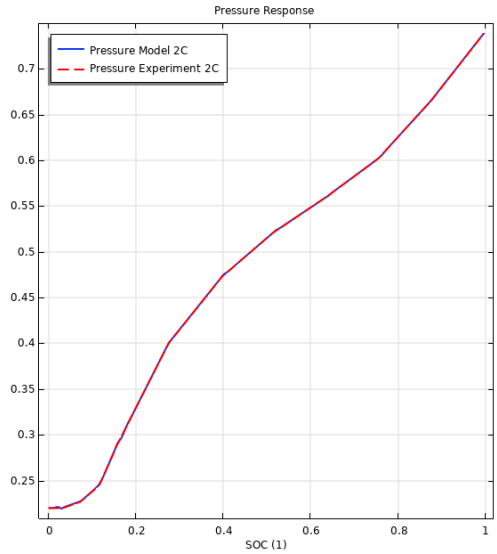


(b) Pressure data comparison with the model for 2C.

Figure 4.15

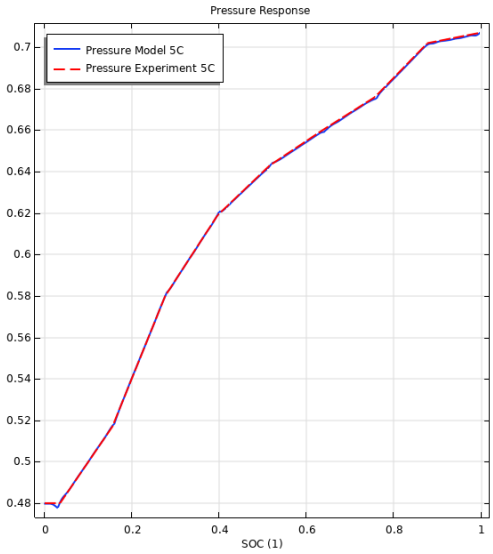


(a) Pressure data comparison with the model for 5C.

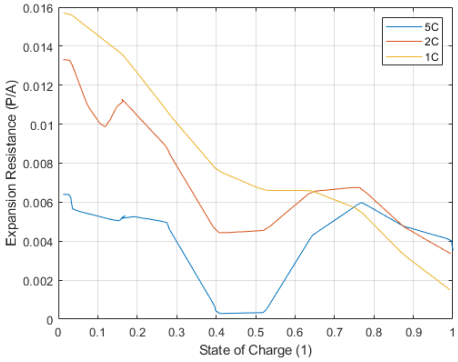


(b) $\mathfrak{R}$ value comparison for the different c-rates.

Figure 4.16

### 4.3.2 Paper 2: Significance of dynamic thickness changes and compression effects of commercial lithium-ion spring-braced cells

The second group of researchers states that thickness change can be categorized into two types [2]. One is reversible where cell thickness changes in an oscillating pattern due to charging and discharging while the other is irreversible where Li-ion plating on the current collector or the SEI layer formation can cause the expansion. This second paper also uses c-rates close to the ones used in this thesis. The experimental values from the paper and model are shown in figure 4.17a, 4.17b and 4.18a. Note however that these have also been used to calculate the $\mathfrak{R}$-values and as such again the error will be zero. Notably, the values of the expansion resistance $\mathfrak{R}$ in figure 4.18b follow a very similar pattern as how they do for this thesis. Note however that for 1C the expansion resistance increases more than the rest at higher SOC, potentially because of Li-ion plating inside the cell.[2]

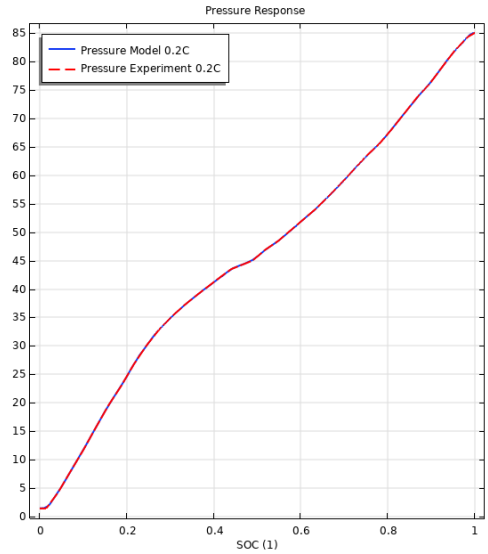


(a) Pressure data comparison with the model for 0.2C.

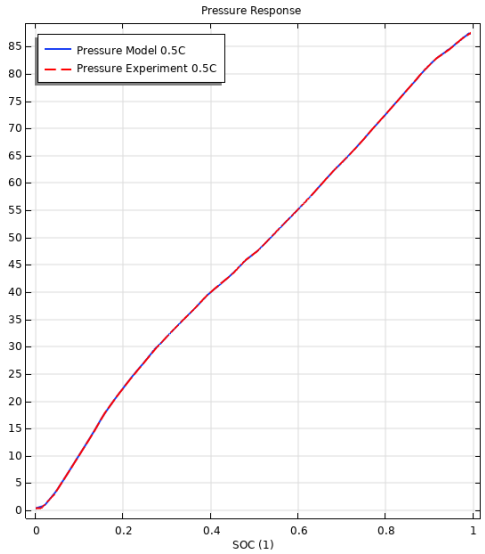


(b) Pressure data comparison with the model for 0.5C.

Figure 4.17

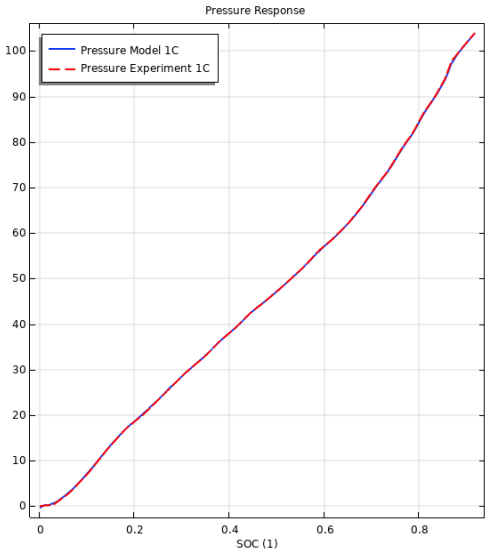


(a) Pressure data comparison with the model for 1C.

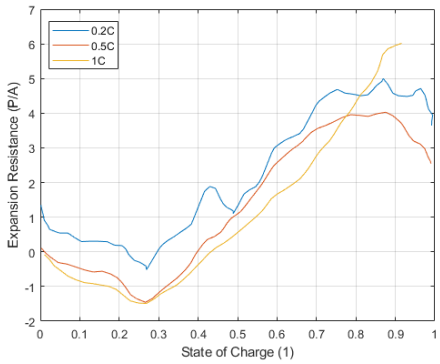


(b) Value comparison of the $\mathfrak{R}_{mech}$ values for the different c-rates.

Figure 4.18

# Chapter 5

# Conclusions

In this chapter, the conclusions from the results as well as future work that might be done are reported.

## 5.1 Results

### 5.1.1 Initial Experiments

There seems to be some c-rate dependency on the pressure change at a charge as well as discharge. However, it seems to change depending on if the experimental c-rate is above or below 0.5C. Below 0.5C the trend is that an increasing c-rate leads to a higher amount of swelling probably due to an increased rate of Li-ion intercalation. Above 0.5C the opposite is seen, with a higher c-rate yielding a smaller pressure change. The latter is however probably due to the test-rig used, where the swelling is not accurately measured at a higher c-rate due to reasons such as the spring effect from the elasticity of the plate that was used, and localized swelling in the center.

For low c-rates the pressure and voltage derivatives with respect to SOC yield two peaks that can be observed for both pressure and voltage, while at higher c-rates two peaks are observed for the pressure and only one for the voltage. It can be assumed that the first peak in both voltage and pressure derivative indicates some kind of phase transformation in the graphite anode probably due to Li intercalation. The second peak that can be observed in the pressure derivatives could also be due to lithium intercalation, but at a higher SOC than the voltage response due to a possible time delay between the voltage and mechanical response of the cell.

### 5.1.2 Modelling

The $\mathfrak{R}$ values as a function of SOC show a clear trend with c-rate, with increasing c-rate leading to smaller $\mathfrak{R}$ values. The shapes of the curves are also conserved with increasing c-rate. Comparing these results to validation data from [18] and[2] it can be concluded that the resistance values follow a clear trend in these cases. In the case of [18], higher c-rates are used compared to the c-rates used in this thesis, as such it is difficult to compare to data in this thesis. There is still a trend in the calculated $\mathfrak{R}$ values, however, it is different and decreases with increasing c-rate. This is however probably due to the c-rate being much higher than what is looked at in this thesis and should not be taken into much consideration. The second paper, [2], uses c-rates closer to what is used in this thesis, and the trends seen in the $\mathfrak{R}$ are more closely emulating the values obtained in this thesis. The increase at the end for 1C in this paper is attributed to Li plating.

## 5.2 Future work and improvement

As previously discussed, there are a lot of things that could be either improved or expanded upon in a future, similar work.

First and foremost the test-rig used is not optimal for swelling experiments with a prismatic cell. Because the swelling in a prismatic Li-ion cell predominantly takes place in the center of the cell and the load sensors were situated at the corners in the test-rig, the exact pressure development was not captured for the higher c-rates, for which a greater swelling than at smaller c-rates should have probably been observed based on previous papers such as [18]. In future work, it would therefore be a good idea to place a load cell in the center of the test-rig, at the center of the cell, where the swelling is the greatest. This would also limit the possibility of unevenness in the measurements. This would most probably improve the experimental results greatly.

Moreover, there's an improvement to be made when it comes to the experimental set-up outside the test-rig. To be sure that the ambient temperature of the cell stays the same, and also in order to decouple thermal effects, it would be a good idea to use a thermal chamber. In this way, the ambient temperature would be regulated therefore allowing a better understanding of the thermal effects that might play a role in the pressure evolution of the cell, especially at higher c-rates. Additionally, it could be a good idea to do testing with different initial external pressures to see how it might affect the swelling of the cell since the external pressure on the cell can affect its lifespan[18].

Furthermore, only the pressure behavior at the beginning of life is studied and modeled, however, it might be interesting to do similar experiments and modeling throughout the aging of the cell, thus eventually obtaining another way to measure the aging of a cell by monitoring its pressure, which could be important in a battery module for example, limiting the possibility of it catastrophically swelling and being destroyed. In the end, this kind of experiment could yield an aging model for the cells' state of health.

Lastly, the analysis has possible improvements including the method in which the SOC is calculated. Now it is assumed that before each charge, the SOC is at 0% SOC regardless of which voltage the cell has relaxed to, which might not be good since the relaxed voltage before the charge will change depending on the c-rate. There is also no constant voltage step after 4.2 $V$ has been reached, which means that we might not actually have reached 100% SOC. Additionally, the calculation is done with simple coulomb counting which can be improved, using better methods for example using a Kálmán filter. Additionally, longer relaxation periods could be used before and after each test in order to make sure that the cell was in a relaxed state. There is also improvement to be done in the calculation of the $\mathfrak{R}_{mech}$, which as of now have all effects: thermal, c-rate, initial external pressure, etc., lumped together. It makes sense to try to decouple these different effects and thus in the end have a more dynamic model.

# Appendices

# Appendix A

# Supplementary Data

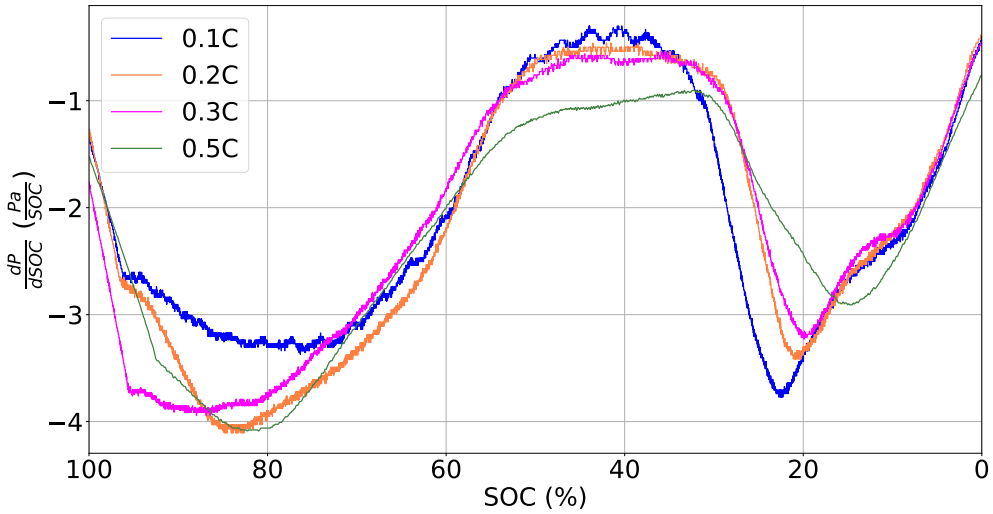


Figure A.1: The pressure derivative with respect to SOC for the discharge from 0.1C to 0.5C.

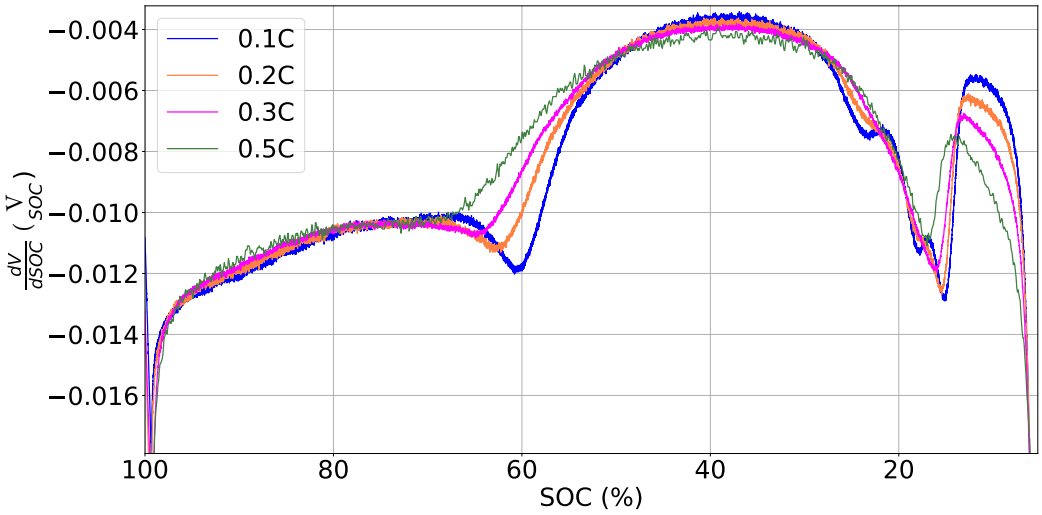


Figure A.2: The Voltage derivative with respect to SOC for the discharge from 0.1C to 0.5C.

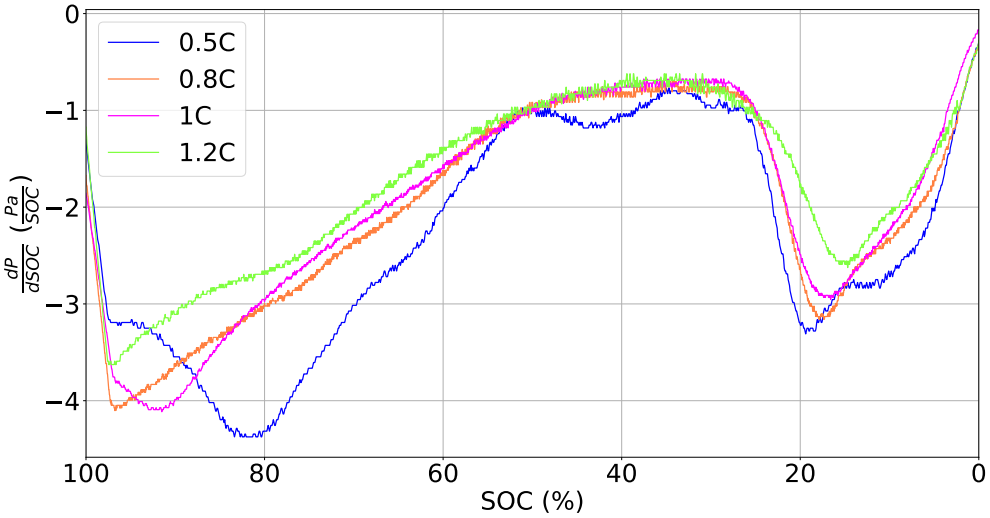


Figure A.3: The pressure derivative with respect to SOC for the discharge from 0.5C to 1.2C.

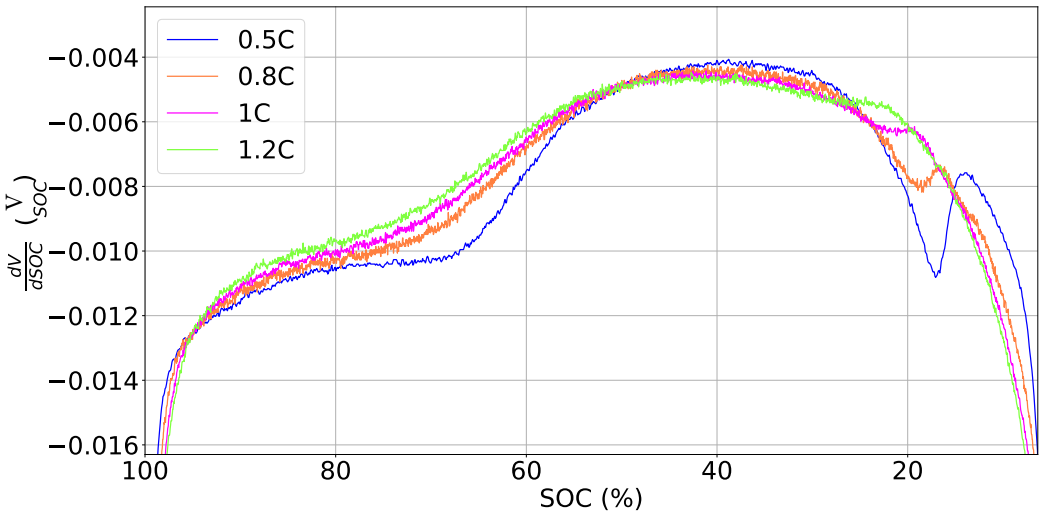


Figure A.4: The Voltage derivative with respect to SOC for the discharge from 0.5C to 1.2C.

# Bibliography


[1] Ki-Yong Oh, Jason B. Siegel, Lynn Secondo, Sun Ung Kim, Nassim A. Samad, Jiawei Qin, Dyche Anderson, Krishna Garikipati, Aaron Knobloch, Bogdan I. Epureanu, Charles W. Monroe, and Anna Stefanopoulou. Rate dependence of swelling in lithium-ion cells. *Journal of Power Sources*, 267:197–202, 2014.

[2] Niklas P. Penningh, Mozaffar Abdollahifar, Peter Michalowski, Wolfgang Haselrieder, and Arno Kwade. Significance of dynamic thickness changes and compression effects of commercial lithium-ion spring-braced cells. *Journal of Energy Storage*, 72:108187, 2023.

[3] Mehrdad Ehsani, Yimin Gao, Stefano Longo, and Kambiz M Ebrahimi. *Modern electric, hybrid electric, and fuel cell vehicles*. CRC press, 2018.

[4] FA Omonov, QM Dehqonov, et al. Electric cars as the cars of the future. *Eurasian Journal of Engineering and Technology*, 4:128–133, 2022.

[5] Aureli Somà, Fabio Bruzzese, Francesco Mocera, and Ezio Viglietti. Hybridization factor and performance of hybrid electric telehandler vehicle. *IEEE Transactions on Industry Applications*, 52(6):5130–5138, 2016.

[6] European Commission. *Proposal for a REGULATION OF THE EUROPEAN PARLIAMENT AND OF THE COUNCIL on type-approval of motor vehicles and engines and of systems, components and separate technical units intended for such vehicles, with respect to their emissions and battery durability (Euro 7) and repealing Regulations (EC) No 715/2007 and (EC) No 595/2009*. 2022.

[7] Francesco Mocera, Elena Vergori, and Aurelio Somà. Battery performance analysis for working vehicle applications. *IEEE Transactions on Industry Applications*, 56(1):644–653, 2019.

[8] Jean-François Cousseau, Clemence Siret, Philippe Biensan, and Michel Broussely. Recent developments in li-ion prismatic cells. *Journal of power sources*, 162(2):790–796, 2006.

[9] Ryan Aalund, Bhavana Endreddy, and Michael Pecht. How gas generates in pouch cells and affects consumer products. *Frontiers in Chemical Engineering*, 4:828375, 2022.

[10] Languang Lu, Xuebing Han, Jianqiu Li, Jianfeng Hua, and Minggao Ouyang. A review on the key issues for lithium-ion battery management in electric vehicles. *Journal of Power Sources*, 226:272–288, 2013.

[11] Kerstin Ryll, Louisa Hoffmann, Oliver Landrath, Frank Lienesch, and Michael Kurrat. Key figure based incoming inspection of lithium-ion battery cells. *Batteries*, 7(1), 2021.

[12] Ching Chuen Chan. The state of the art of electric, hybrid, and fuel cell vehicles. *Proceedings of the IEEE*, 95(4):704–718, 2007.

[13] Seyed Saeed Madani, Erik Schaltz, and Søren Knudsen Kær. Characterization of the compressive load on a lithium-ion battery for electric vehicle application. *Machines*, 9(4):71, 2021.

[14] M Holzapfel, A Würsig, W Scheifele, J Vetter, and P Novák. Oxygen, hydrogen, ethylene and co2 development in lithium-ion batteries. *Journal of Power Sources*, 174(2):1156–1160, 2007.

[15] Yongkun Li, Chuang Wei, Yumao Sheng, Feipeng Jiao, and Kai Wu. Swelling force in lithium-ion power batteries. *Industrial & Engineering Chemistry Research*, 59(27):12313–12318, 2020.

[16] Conner Fear, Daniel Juarez-Robles, Judith A Jeevarajan, and Partha P Mukherjee. Elucidating copper dissolution phenomenon in li-ion cells under over-discharge extremes. *Journal of the Electrochemical Society*, 165(9):A1639, 2018.

[17] Epec Engineered Technologies Build to Print Electronics. Prismatic pouch battery packs. `https://www.epectec.com/batteries/prismatic-pouch-packs.html`. Accessed: 2023-02-09.

[18] Ruicheng Shen, Shaojun Niu, Guobin Zhu, Kai Wu, and Honghe Zheng. Mechanical behavior analysis of high power commercial lithium-ion batteries. *Chinese Journal of Chemical Engineering*, 58:315–322, 2023.

[19] eBay. Toyota prius hybrid battery cell nimh module 2004 2005 2006 2007 2008 2009. `https://www.ebay.com/itm/393355232274`. Accessed: 2023-02-24.

[20] PriusChat. Bulged battery modules? never seen that before. `https://priuschat.com/threads/bulged-battery-modules-never-seen-that-before.181923/`. Accessed: 2023-02-24.

[21] Kazuma Kumai, Hajime Miyashiro, Yo Kobayashi, Katsuhito Takei, and Rikio Ishikawa. Gas generation mechanism due to electrolyte decomposition in commercial lithium-ion cell. *Journal of Power Sources*, 81-82:715–719, 1999.

[22] Seon-Hong Lee and In-Hwan Ko. Failure analysis of swelling in prismatic lithium-ion batteries during their cycle life after long-term storage. *Journal of Failure Analysis and Prevention*, 18:554–561, 2018.

[23] Ki-Yong Oh and Bogdan I. Epureanu. A novel thermal swelling model for a rechargeable lithium-ion battery cell. *Journal of Power Sources*, 303:86–96, 2016.

[24] Ki-Yong Oh, Bogdan I Epureanu, Jason B Siegel, and Anna G Stefanopoulou. Phenomenological force and swelling models for rechargeable lithium-ion battery cells. *Journal of Power Sources*, 310:118–129, 2016.

[25] Davide Clerici, Francesco Mocera, and Aurelio Soma. Electrochemical–mechanical multi-scale model and validation with thickness change measurements in prismatic lithium-ion batteries. *Journal of Power Sources*, 542:231735, 2022.

[26] Priyank Gupta. *Experimental Characterization of Electrodes and Multi-Scale Modeling of Swelling Induced Stresses in Lithium-ion Batteries*. PhD thesis, KTH, Solid Mechanics, 2023. QC 230620.

[27] Abhiram Lakshmipuram Govindaraj. Phenomenological swelling model of battery module. Master's thesis, KTH, Solid Mechanics, 2022.

[28] Jedrzej Piatek, Semih Afyon, Tetyana M Budnyak, Serhiy Budnyk, Mika H Sipponen, and Adam Slabon. Sustainable li-ion batteries: chemistry and recycling. *Advanced Energy Materials*, 11(43):2003456, 2021.

[29] I Riess. What does a voltmeter measure? *Solid State Ionics*, 95(3-4):327–328, 1997.

[30] Joe C Stallard, Laura Wheatcroft, Samuel G Booth, Rebecca Boston, Serena A Corr, Michael FL De Volder, Beverley J Inkson, and Norman A Fleck. Mechanical properties of cathode materials for lithium-ion batteries. *Joule*, 2022.

[31] Mark Brehob, R.J. Enbody, Young-Kyun Kwon, and David Tomanek. The potential of carbon-based memory systems. pages 110 – 114, 02 1999.

[32] Izumi Umegaki, Shigehiro Kawauchi, Hiroshi Sawada, Hiroshi Nozaki, Yuki Higuchi, Kazutoshi Miwa, Yasuhito Kondo, Martin Mansson, Mark Telling, Fiona Coomer, Stephen Cottrell, Tsuyoshi Sasaki, Tetsuro Kobayashi, and Jun Sugiyama. Li-ion diffusion in li intercalated graphite c6li and c12li probed by +sr. *Physical Chemistry Chemical Physics*, 19:–, 07 2017.

[33] Chaofeng Liu, Zachary G Neale, and Guozhong Cao. Understanding electrochemical potentials of cathode materials in rechargeable batteries. *Materials Today*, 19(2):109–123, 2016.

[34] Andre Pierre Legrand and A Flandrois. *Chemical Physics of interccalation*, volume 172. Springer Science & Business Media, 2013.

[35] Rosamaria Fong, Ulrich Von Sacken, and Jeff R Dahn. Studies of lithium intercalation into carbons using nonaqueous electrochemical cells. *Journal of The Electrochemical Society*, 137(7):2009, 1990.

[36] Martin Winter, Jürgen O Besenhard, Michael E Spahr, and Petr Novak. Insertion electrode materials for rechargeable lithium batteries. *Advanced materials*, 10(10):725–763, 1998.

[37] Naoki Nitta, Feixiang Wu, Jung Tae Lee, and Gleb Yushin. Li-ion battery materials: present and future. *Materials today*, 18(5):252–264, 2015.

[38] Matthew Li, Jun Lu, Zhongwei Chen, and Khalil Amine. 30 years of lithium-ion batteries. *Advanced Materials*, 30(33):1800561, 2018.

[39] wattalps. Lithium-ion positive electrode technologies. `https://www.wattalps.com/lithium-ion-positive-electrode-technologies/`.

[40] Quan-Qing Yu, Rui Xiong, Le-Yi Wang, and Cheng Lin. A comparative study on open circuit voltage models for lithium-ion batteries. *Chinese Journal of Mechanical Engineering*, 31(1):1–8, 2018.

[41] John B Goodenough and Youngsik Kim. Challenges for rechargeable li batteries. *Chemistry of materials*, 22(3):587–603, 2010.

[42] Bo Lu, Yicheng Song, Qinglin Zhang, Jie Pan, Yang-Tse Cheng, and Junqian Zhang. Voltage hysteresis of lithium ion batteries caused by mechanical stress. *Phys. Chem. Chem. Phys.*, 18:4721–4727, 2016.

[43] Mengyun Nie, Dinesh Chalasani, Daniel P Abraham, Yanjing Chen, Arijit Bose, and Brett L Lucht. Lithium ion battery graphite solid electrolyte interphase revealed by microscopy and spectroscopy. *The Journal of Physical Chemistry C*, 117(3):1257–1267, 2013.

[44] Tsutomu Ohzuku, Yasunobu Iwakoshi, and Keijiro Sawai. Formation of lithium-graphite interccalation compounds in nonaqueous electrolytes and their application as a negative electrode for a lithium ion (shuttlecock) cell. *Journal of The Electrochemical Society*, 140(9):2490, 1993.

[45] Simon Schweidler, Lea de Biasi, Alexander Schiele, Pascal Hartmann, Torsten Brezesinski, and Jurgen Janek. Volume changes of graphite anodes revisited: a combined operando x-ray diffraction and in situ pressure analysis study. *The Journal of Physical Chemistry C*, 122(16):8829–8835, 2018.

[46] Oleksandr Dolotko, Anatoliy Senyshyn, MJ Mühlbauer, Kristian Nikolowski, and Helmut Ehrenberg. Understanding structural changes in nmc li-ion cells by in situ neutron diffraction. *Journal of Power Sources*, 255:197–203, 2014.

[47] Lea de Biasi, Aleksandr O Kondrakov, Holger Geßwein, Torsten Brezesinski, Pascal Hartmann, and Jurgen Janek. Between scylla and charybdis: balancing among structural stability and energy density of layered ncm cathode materials for advanced lithium-ion batteries. *The Journal of Physical Chemistry C*, 121(47):26163–26171, 2017.

[48] Karen E Thomas and John Newman. Heats of mixing and of entropy in porous insertion electrodes. *Journal of power sources*, 119:844–849, 2003.

[49] Kaiwei Chen, Grant Unsworth, and Xianguo Li. Measurements of heat generation in prismatic li-ion batteries. *Journal of Power Sources*, 261:28–37, 2014.

[50] Zeyang Geng. *Characterization Methods and Modelling for Li-Ion Batteries: Entropy, Impedance, Pressure, Diffusivity & Temperature Swings Induced Aging*. Chalmers Tekniska Hogskola (Sweden), 2022.

[51] Peyman Taheri, Abraham Mansouri, Maryam Yazdanpour, and Majid Bahrami. Theoretical analysis of potential and current distributions in planar electrodes of lithium-ion batteries. *Electrochimica Acta*, 133:197–208, 2014.

[52] Helena Berg. *Cell design*, page 126–140. Cambridge University Press, 2015.

[53] Ltd. Murata Manufacturing Co. Cylindrical type lithium ion secondary batteries. https://www.murata.com/en-global/products/batteries/cylindrical. Accessed: 2023-02-15.

[54] Bingbin Wu, Yang Yang, Dianying Liu, Chaojiang Niu, Mark Gross, Lorraine Seymour, Hongkyung Lee, Phung ML Le, Thanh D Vo, Zhiqun Daniel Deng, et al. Good practices for rechargeable lithium metal batteries. *Journal of The Electrochemical Society*, 166(16):A4141, 2019.

[55] OSN Power Energy Limited. High discharge rate 5c customized pouch 3.7v nmc li-ion 30ah cells. https://www.osnpower.com/high-discharge-rate-5c-customized-pouch-3-7v-nmc-li-ion-30ah-cells_p62.html. Accessed: 2023-02-16.

[56] Made in China. [hot item] rechargeable lifepo4 a123 3.2v 15ah 20ah 30ah prismatic pouch cell. https://ubetterbattery.en.made-in-china.com/product/cjZJYkMvEVWm/China-Rechargeable-LiFePO4-A123-3-2V-15ah-20ah-30ah-Prismatic-Pouch-Cell.html. Accessed: 2023-02-16.

[57] The MathWorks Inc. Matlab version: 9.13.0 (r2022b), 2022.

[58] COMSOL Multiphysics. Introduction to comsol multiphysics®. *COMSOL Multiphysics, Burlington, MA, accessed Feb*, 9:2018, 1998.

[59] Gabriel Hassellöf Johannes Karlsson Emil Blomster, Louise Bohl. Höjdförändring i ett li-jon batteri. 2021.

[60] Fc23 compression load cell. https://www.te.com/commerce/DocumentDelivery/DDEController?Action=showdoc&DocId=Data+Sheet%7FFC23%7FA%7Fpdf%7FEnglish%7FENG_DS_FC23_A.pdf%7FCAT-FSE0002. Accessed: 2023-03-02.

[61] LISAB Load indicator system ab. Lcb by lisab, 2023.

[62] Ipetronik msens-2. https://www.ipetronik.com/files/products/M-SENS%202_datasheet_en.pdf. Accessed: 2023-03-02.

[63] MACCOR. Series 4000 automated test system. http://www.maccor.com/ProductDocs/Data%20Sheet%20for%20Series%204000%20Test%20System.pdf.

[64] Ankit Rohatgi. Webplotdigitizer: Version 4.6, 2022.

[65] ZX Shu, RS McMillan, and JJ Murray. Electrochemical intercalation of lithium into graphite. *Journal of The Electrochemical Society*, 140(4):922, 1993.

[66] Sou Taminato, Masao Yonemura, Shinya Shiotani, Takashi Kamiyama, Shuki Torii, Miki Nagao, Yoshihisa Ishikawa, Kazuhiro Mori, Toshiharu Fukunaga, Yohei Onodera, et al. Real-time observations of lithium battery reactions—operando neutron diffraction analysis during practical operation. *Scientific reports*, 6(1):28843, 2016.